Chapter 3
Porphyrins: Syntheses and Properties

Jun-ichiro Setsune

Abstract It is well known that *meso*-tetraarylporphyrins are obtained readily by condensation reactions between pyrroles and aromatic aldehydes. The 2+2 type condensation of aryldipyrrylmethanes and the second aromatic aldehyde is useful for synthesizing porphyrins with mixed *meso*-aryl groups, and further transformations of the porphyrin periphery are performed conveniently by using organometallic methodology. Some *meso*-aryl substituted porphyrins are designed for supramolecular application and photosensitizing effect. Porphyrins substituted at pyrrole β-positions are obtainable by using Barton–Zard synthesis, and these compounds are further converted into benzoporphyrins that are structurally similar to phthalocyanines and play an important role in the development of a variety of photo-functional materials. Porphyrins more heavily π-extended than benzoporphyrin are focused in the last part of this chapter. Multiple porphyrin cores are directly bridged by π-units or aromatic substituents at the porphyrin periphery are forced to come into π-conjugation with the porphyrin π-system by Scholl reactions, leading to strong infrared absorption bands at longer wavelength beyond 1000 nm, very small HOMO–LUMO gap, and very high two-photon absorption efficiency.

3.1 Introduction

Porphyrins are fully π-conjugated macrocycles where four pyrrole rings are connected by sp^2-hybridized carbon atoms. The macrocyclic π-conjugation and the dianionic tetradentate coordination site provide basis for a wide variety of applications. Photophysical, electrochemical, and coordination properties of porphyrins have been drawing great interest in a variety of scientific fields and these properties are tunable by the abundant methodology for structure modification. Comprehensive reviews on the current porphyrin studies have been published as multi-volume reference books (Kadish et al. 2000, 2010; Dolphin 1978). This chapter describes functionalized porphyrins with focusing on their synthetic methodology and their

J. Setsune (✉)
Department of Chemistry, Graduate School of Science, Kobe University, Kobe, Japan
e-mail: setsunej@kobe-u.ac.jp

Y. Ooyama and S. Yagi (eds.), *Progress in the Science of Functional Dyes*,
https://doi.org/10.1007/978-981-33-4392-4_3

properties caused by structural diversity. Although some aspects of application to material science and medicine will be mentioned here, they are arbitrarily selected just for examples. A large number of porphyrin analogues (expanded, contracted, and isomeric porphyrins) have been developed these days and their unusual structure and properties have been adding great insights into the porphyrin chemistry. These subjects have recently been reviewed (Sessler et al. 2017), and not included here.

3.2 *meso*-Tetra-substituted Porphyrins

3.2.1 Condensation of Pyrrole and Aldehyde

meso-Tetraarylporphyrins are produced by simple procedures known as a Rothemund method and a Longo-Adler method (Rothemund 1935; Adler et al. 1967). After heating a mixture of pyrrole and aromatic aldehyde in acetic acid or propionic acid under aerobic conditions, the reaction mixture was left overnight at room temperature to generate crystalline A_4-type porphyrins with D_{4h} symmetry usually in the yields more or less 20%. Since rotation of *meso*-aryl groups with *ortho*-substituents is limited, conformational isomers called atropisomers are separated and their stability is dependent on the bulkiness of the *ortho*-substituents. Collman's group constructed an O_2-binding heme model by using an αααα-isomer of *meso*-tetra(*o*-aminophenyl)porphyrin **2** that was obtained by condensation of pyrrole and *ortho*-nitrobenzaldehyde followed by $SnCl_2$ reduction (Collman et al. 1975). **2** is regarded as a scaffold for molecular architecture of unique stereochemistry (Fig. 3.1). Four possible atropisomers (αααα, ααββ, αααβ, αβαβ) occur at equilibrium in a 1:2:4:1 statistical ratio, but Lindsey found that the αααα isomer with all four amino groups on the same face of the porphyrin plane was obtained in 66% yield after heating the benzene solution of the equilibrium mixture in the presence of silica gel due to

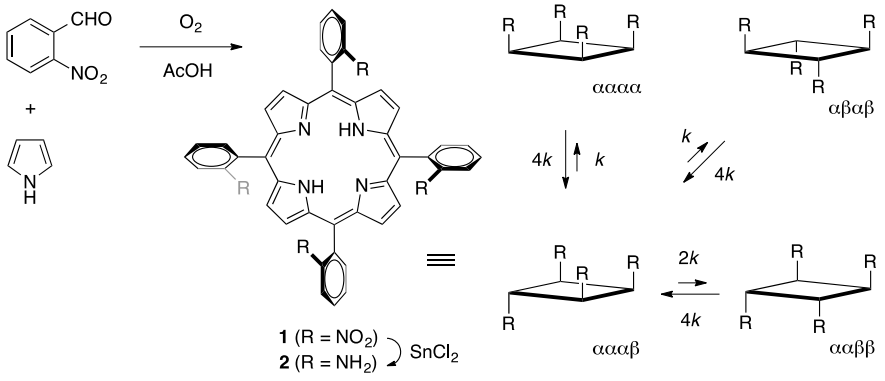

Fig. 3.1 Atropisomerism of *meso*-tetraarylporphyrins

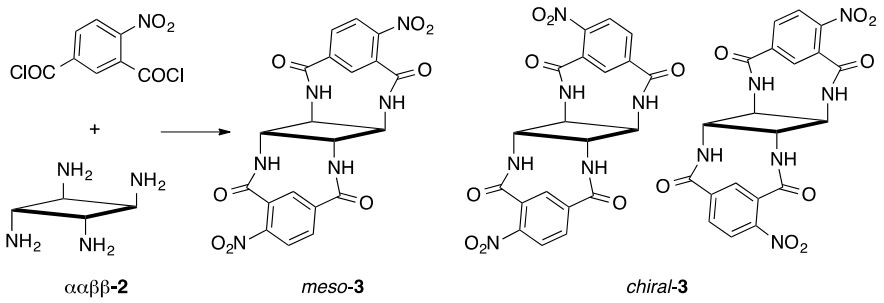

Fig. 3.2 Chiral porphyrins derived from *meso*-tetraarylporphyrins

the preferential adsorption of the target isomer (Lindsey 1980). On the other hand, Nishino reported that the αβαβ atropisomer of *meso*-tetra(*o*-nitrophenyl)porphyrin **1** could be enriched in refluxing toluene (Nishino et al. 1992). Therefore, equilibration in toluene at reflux followed by reduction and chromatographic separation produced 52% yield of the pure αβαβ atropisomer of **2**.

Unsymmetrical bridges were introduced into the ααββ-isomer of *meso*-tetra(*o*-aminophenyl)porphyrin **2** to give a 1:1 mixture of *meso*-**3** and *chiral*-**3** in the studies on molecular recognition by Ogoshi, Kuroda, and coworkers (Fig. 3.2) (Kuroda et al. 1995). The *chiral*-**3** was separated into a C_2-symmetric enantiomer pair by HPLC on a chiral phase and the binding constants of their Zn complexes toward amino acid esters were dependent on the chirality of the enantiomeric porphyrins with sevenfold difference.

Sugiura, Sakata, and coworkers separated A_3B-type porphyrin **4** and A_2B_2-type porphyrin **5** in 12% and 3% yield, respectively, from a mixture of porphyrin products in the mixed condensation of pyrrole with two different aromatic aldehydes under Longo–Adler reaction conditions (Fig. 3.3) (Sugiura et al. 1999). The ester groups of **4** and **5** were converted into formyl groups and then subjected to the mixed condensation with pyrrole again to give the pentameric porphyrin **6** in 25% yield using Lindsey's protocol for hindered porphyrins. That is, a one-flask two-step procedure of acid-catalyzed condensation at room temperature in highly diluted CH_2Cl_2 solution followed by DDQ oxidation of the porphyrinogen intermediate (**7** in Fig. 3.4) (Lindsey et al. 1987). The pentamer **6** was utilized as a precursor to the dendritic molecular architecture composed of 21 porphyrin nuclei and 64 benzene units through the condensation with pyrrole under Lindsey conditions. The final product was obtained in 44% yield and its molecular image was actually observed by STM as a square shape of 65 Å along the sides that is consistent with the theory 65.7 Å.

Mixed condensations are an easy way to functional porphyrins such as used for chirality sensors. Nakanishi and Berova had pointed out that the exciton coupling of two porphyrins in a skewed conformation gives a strong CD couplet at the Soret band region at ca. 400 nm and its sign is diagnostic of the absolute configuration of the optically active guests that was bound cooperatively to the two porphyrin units (Huang

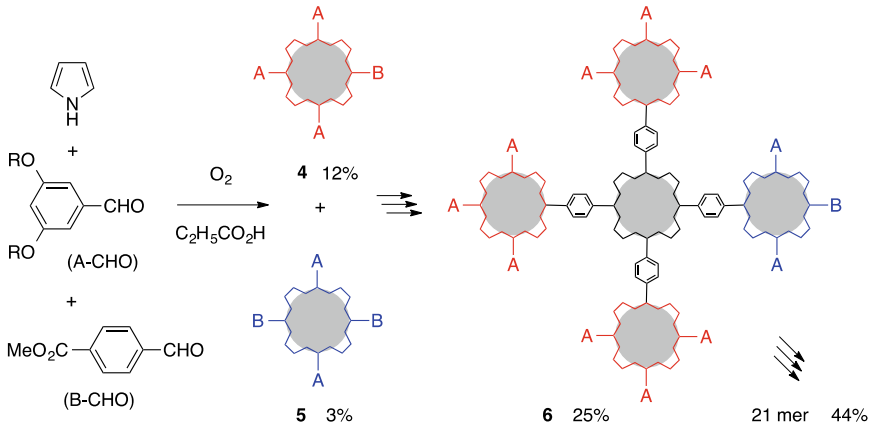

Fig. 3.3 Synthesis of square-shaped porphyrin oligomers

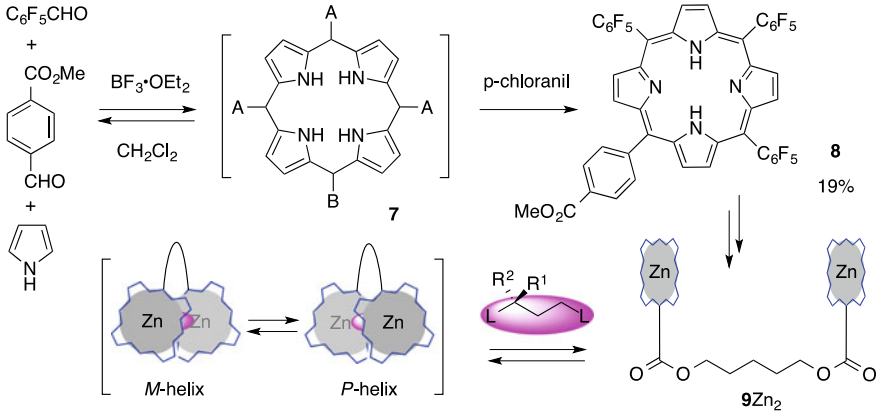

Fig. 3.4 Direct synthesis of A_3B-type *meso*-tetraarylporphyrin and its application to diporphyrin

et al. 1998). Their molecular design of the diporphyrin chiral sensor was modified by Borhan and coworkers. The mixed condensation of pentafluorobenzaldehyde, 4-carbomethoxybenzaldehyde, and pyrrole in the molar ratio of 3:1:4 according to Lindsey's protocol afforded 19% yield of A_3B-type porphyrin **8** after chromatographic separation of a mixture of porphyrin products with statistical distribution of *meso*-aryl substitution pattern (Fig. 3.4) (Li et al. 2008). **8** was converted to Zn porphyrin dimer **9**Zn_2 which was used for chirality sensing of optically active guest molecules such as diamines, aminoalcohols, and dialcohols. *meso*-Pentafluorophenyl groups increased Lewis acidity of Zn(II) and the guest binding was dependent on the chain length of the linker. Binding of the asymmetric guest molecules to **9**Zn_2 induces face-to-face orientation of two porphyrin rings with their electronic transition

moments in a skewed orientation. Thus, chirality of the guest molecule is translated into the helicity of the host molecule.

3.2.2 *Lindsey Synthesis Using Dipyrrylmethanes*

The above-mentioned Lindsey protocol of acid-catalyzed condensation followed by oxidation is applicable to selective formation of *trans*-A_2B_2-type porphyrin **11** from aryldipyrrylmethanes **10** and the second aromatic aldehyde (Fig. 3.5) (Ravikanth et al. 1998). But it should be remembered that decomposition of **10** and a porphyrinogen intermediate to pyrrole and aromatic aldehyde is also acid-catalyzed to result in scrambling of the *meso*-aryl substitution pattern in the porphyrin products. Lindsey also reported an alternative route to **11** under milder reaction conditions taking advantage of more reactive intermediate, aryldipyrrylmethane-2,9-dicarbinol **13′** that is effectively obtained by sequential reactions of **10** with aroyl chloride and $NaBH_4$ (Zaidi et al. 2006). This synthetic method using aryldipyrrylmethane and aryldipyrrylmethane-2,9-dicarbinol was applied to A_3B-type porphyrins and AB_2C-type porphyrins. Since aryldipyrrylmethane-2,9-dicarbinol with three different aryl groups **13** was prepared by way of monoacylation of **10** with 2-pyridyl thioester under low temperature, ABCD-type porphyrins **14** were also prepared (Rao et al. 2000; Lindsey 2010).

Dimeric AB_2C-type porphyrin **15** that is known as a gable porphyrin was designed so as to make supramolecular cyclic assembly of six units (Fig. 3.6) (Takahashi and Kobuke 2005). Kobuke and coworkers obtained 2% yield of **15** through

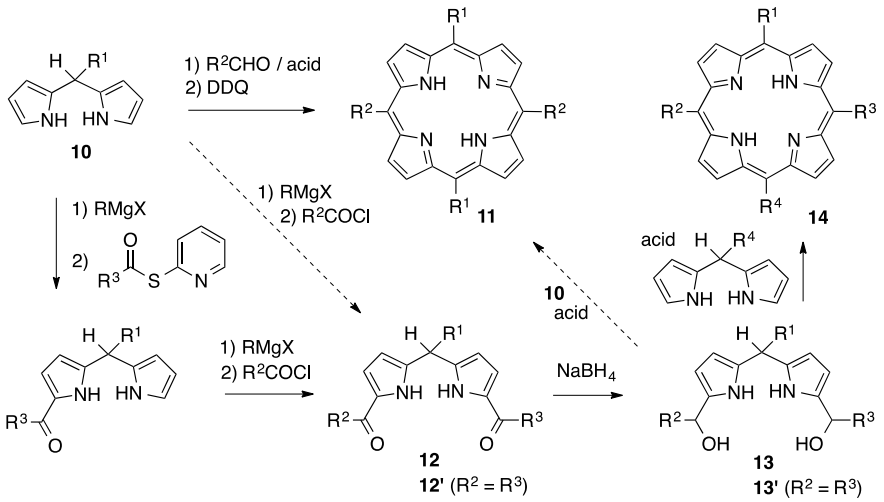

Fig. 3.5 Synthetic routes to *meso*-tetraarylporphyrins of various substitution patterns

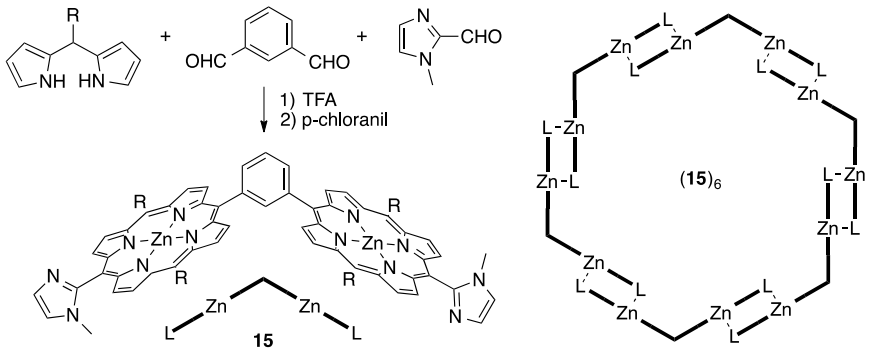

Fig. 3.6 Synthesis of a gable porphyrin for modeling a light-harvesting complex

TFA-catalyzed mixed condensation of 5-alkyldipyrrylmethane, 1-methylimidazole-2-aldehyde, and isophthalaldehyde. Since preparation yields in the single porphyrin ring-forming reaction which is usually less than 20%, double porphyrin ring-forming reactions would be very low and separation of the target porphyrin is problematic. Reversible coordination of imidazole to Zn allowed reorganization into the cyclic oligomers of 12 porphyrin units. The dimeric porphyrin units of a slipped cofacial orientation constituting the macro ring assembly (**15**)$_6$ showed close analogy to the dimeric chlorophyll units assembled in the light-harvesting complexes of photosynthetic bacteria.

Aida and coworkers reported A_2B_2-type porphyrin **16** in 13% synthetic yield and A_3B-type porphyrin as a byproduct in 4% yield through acid-catalyzed condensation of 5-(2,6-dimethoxyphenyl)-2,3,7,8-tetramethyldipyrrylmethane and benzaldehyde (Fig. 3.7) (Mizuno et al. 2000). The fully substituted porphyrin **16** undergoes a saddle shape distortion of the porphyrin plane in order to relieve steric crowding in its periphery, which results in the introduction of chirality. Although these enantiomeric forms, (*M*, *M*)- and (*P*, *P*)-form, interconvert rapidly by macrocyclic inversion at room temperature, this conformational change slowed down when they bind two molecules of carboxylic acids. If optically active guests were bound, either one of the diastereomeric pair is favored. For example, a strong CD signal in the negative sign was generated in the visible region (450–500 nm) when (*S*)-mandelic acid was added to **16** to lead to very high (>98%) diastereoselectivity. Thus, absolute configuration of optically active acids can be determined by the CD Cotton effect due to the porphyrin chromophore. When these diastereomerically biased adducts were dissolved in acetic acid, the chiral guests were replaced by acetic acids to generate enantiomerically biased adducts, the optical purity of which lasts in the timescale of days.

In addition to this chiral memory phenomenon, photoresponsive change in optical purity of the (*S*)-mandelic acid adduct of **16** was reported in on–off cycles of irradiation of the Soret band. That is, light irradiation caused racemization and the favored original diastereomeric adduct was reassembled in the dark. Crystals generated from

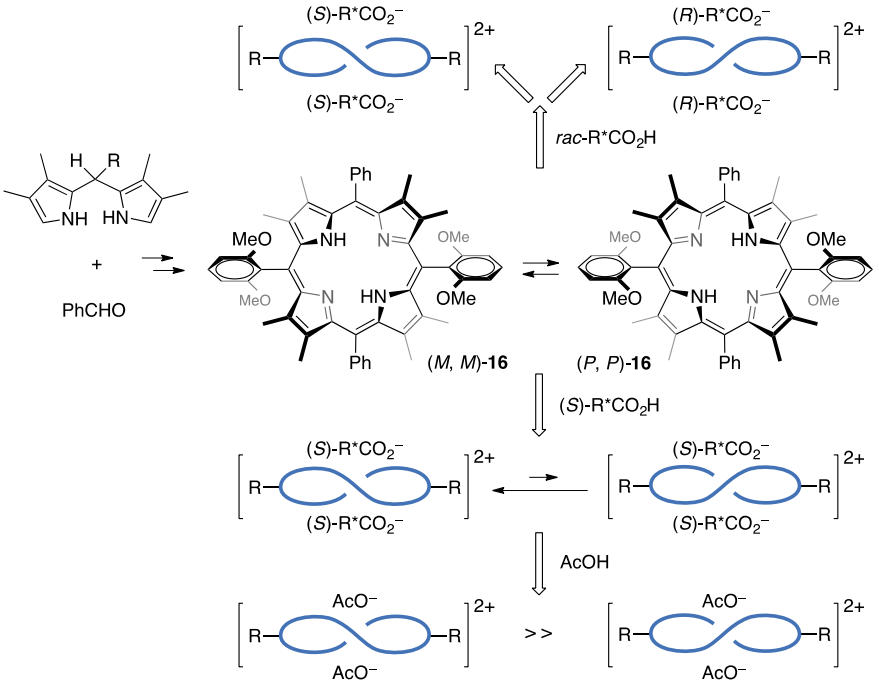

Fig. 3.7 Chirality sensing and optical resolution of carboxylic acids by using *trans*-A_2B_2-type *meso*-tetraarylporphyrin of D_2 symmetry

a solution of a mixture of **16** and racemic mandelic acid derivatives (1:2.1) were found to be a conglomerate leading to spontaneous optical resolution of the guests (Mizuno et al. 2006).

3.2.3 Porphyrins with Mixed meso*-Substituents*

A variety of porphyrins of various *meso*-substitution patterns can be derivatized from readily available simple porphyrins by introducing *meso*-substituents and their further transformation as demonstrated by Senge and coworkers (Fig. 3.8) (Senge 2011). *trans*-A_2-type *meso*-diarylporphyrins **18** are synthesized conveniently by Lindsey protocol of reacting an equimolar mixture of dipyrrylmethane **17** and aromatic aldehyde with TFA (0.1 equiv) in CH_2Cl_2 followed by DDQ (2 equiv) oxidation. The preparation yields of this 2+2 condensation sometimes amount to ~50% when aromatic aldehydes are not sterically demanding (Senge et al. 2010). Mixed condensation of **17** affords *trans*-AB-type *meso*-diarylporphyrins **19**, for example, 5-*p*-tolyl-15-*o*-anisylporphyrin was prepared in 22% yield (Fig. 3.8) (Senge et al. 2011). Simple procedures for **18** and **19** in relatively good yields provide a practical approach

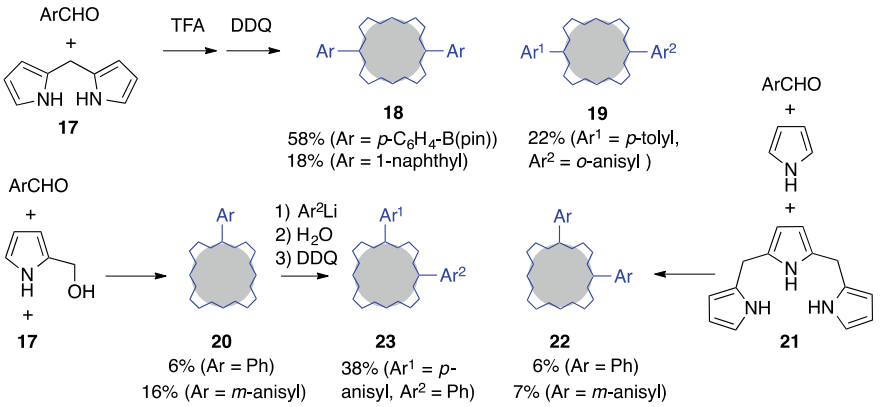

Fig. 3.8 Synthesis of A-type, A_2-type, and AB-type porphyrins

to various *meso*-substituted porphyrins. *cis*-A_2-type *meso*-diarylporphyrins **22** was synthesized by the 3+1 condensation of tripyrrane **21**, pyrrole, and aromatic aldehyde in the molar ratio of 1:1:2, for example, 5,10-diphenylporphyrin was prepared in 6% yield. The 2+1+1 condensation of 2-hydroxymethylpyrrole, **17**, and aromatic aldehyde gave A-type *meso*-arylporphyrins **20** that can be converted into *cis*-AB-type *meso*-diarylporphyrins **23** by nucleophilic addition of organolithium reagents (Ryppa et al. 2005).

Porphyrin *meso*-positions undergo ordinary electrophilic substitution reactions such as formylation, nitration, halogenation, and so on. Furthermore, various substituents can be introduced into the *meso*-position of porphyrin by means of transition metal-catalyzed cross-coupling reactions (Fig. 3.9) (Senge 2011; Ryan et al. 2011). *trans*-AB-type *meso*-diarylporphyrins **19** was readily brominated to

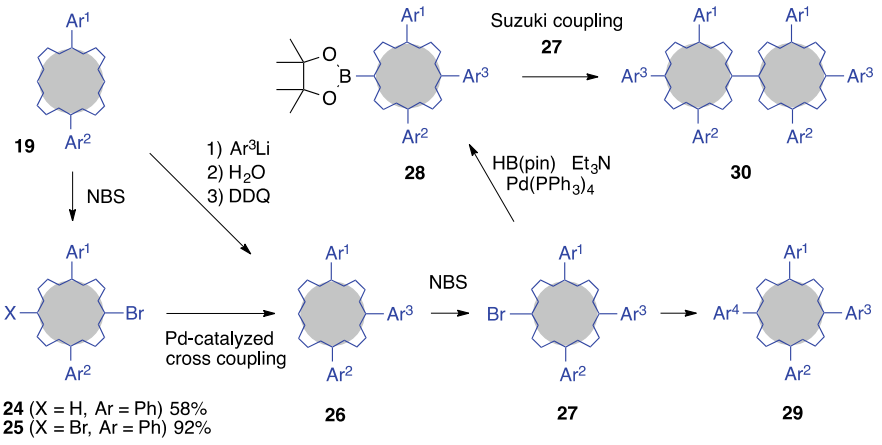

Fig. 3.9 Post-introduction of *meso*-substituents into porphyrin

afford monobromo compound **24** and dibromo compound **25** in good yields. These porphyrins can be subjected to various Pd- or Ni-catalyzed cross-coupling reactions to introduce (hetero)aromatic units by Suzuki coupling and Stille coupling, alkynyl units by Sonogashira coupling, vinyl units by Mizorogi-Heck reaction, and amines by Buchwald–Hartwig reaction. ABC-type *meso*-triarylporphyrins **26** are obtained in good yields in this way from **24,** and these porphyrins were prepared directly from **19** in good yields through the S_NAr reaction. It is noteworthy that alkyllithium reagents work well to introduce a *meso*-alkyl substituent that is relatively difficult to achieve by metal-catalyzed cross-coupling reactions. The iterative procedures starting from **26** afforded ABCD-type *meso*-tetraarylporphyrins **29**. Dioxaborolanylporphyrin **28** was readily prepared by Pd-catalyzed borylation of bromoporphyrin **27** with pinacolborane (HB(pin)), and it was employed as a coupling partner in the Suzuki coupling, for example, symmetrical *meso,meso*-linked diporphyrin **30** was synthesized.

3.2.4 meso-*Substituted Porphyrins as Photosensitizers*

Figure 3.10 illustrates synthesis of a photosensitizer, YD2-*o*-C8, that showed remarkable solar-to-electric power conversion efficiency (PCE) as used in the dye-sensitized solar cell (DSSC) known as a Grätzel cell (Yella et al. 2011). Since the 11.9% PCE under standard air mass 1.5 G illumination exceeds that of DSSC based on the ruthenium sensitizers, push–pull type porphyrin structures with electron-donating substituents and electron-withdrawing substituents arranged at the periphery are extensively studied. These structures are believed to enhance

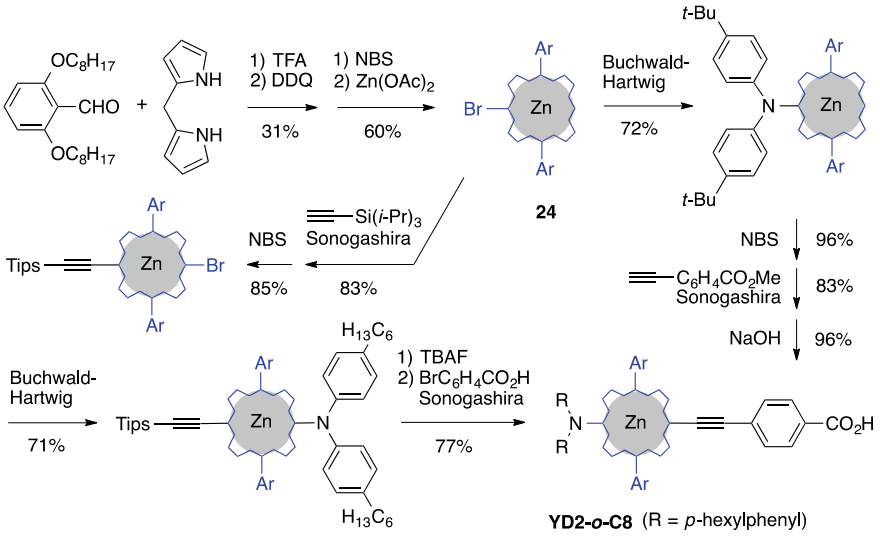

Fig. 3.10 Synthesis of *trans*-A_2BC-type push–pull porphyrins

Table 3.1 Power conversion efficiency (PCE) of Grätzel cell with porphyrin photosesitizers

Photosesitizer	PCE (%)	Ar	R	x	y
YD2-*o*-C8	11.9	2,6-di-octyloxy-phenyl	hexyl	0	1
GY50	12.8			1	1
GY21	2.5			1	0
SM315	13.0		2,4-di-hexyloxy-phenyl	1	1
SM371	12.0			0	1
YD2	8.4	3,5-di-*t*-butylphenyl	hexyl	0	1
ZnPBAT	>YD2	–	–	1	–
ZnPBA	YD2>	–	–	0	–

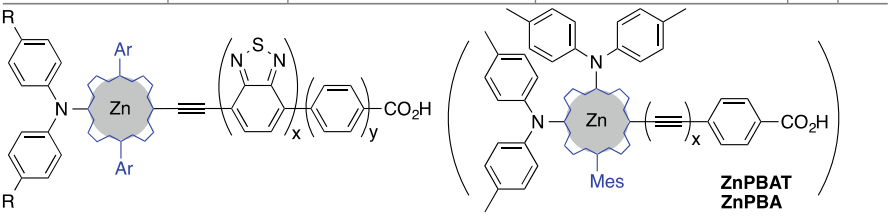

light-harvesting property that is originated from the intense absorption bands of porphyrins extending from visible to NIR region. Furthermore, introduction of long-chain alkoxy groups was suggested to help suppressing charge recombination process. The Grätzel's group prepared the *trans*-A_2BC type porphyrin, YD2-*o*-C8, as a photosensitizer through Sonogashira coupling, Buchwald-Hartwig amination, and the second Sonogashira coupling, in sequence starting from 5,15-di(2,6-dioctyloxyphenyl)-10-bromoporphyrin **24**. Senge and coworkers recently proposed Buchwald-Hartwig amination of **24** as the first step leading to a shorter route to this type of porphyrins (Fig. 3.10) (Meindl et al. 2017). The PCE value of 11.9% of YD2-*o*-C8 was greater than 8.4% of the reference dye YD2 under the same conditions using $Co^{II/III}$ tris(bipyridyl) complex as electrolyte (Table 3.1), and their UV–vis absorption spectra have a tailing up to 700 nm with absorption maxima at 442 nm (log ε 5.3), 576 nm (log ε 4.1), and 638 nm (log ε 4.4) in CH_2Cl_2.

If *cis*-A_2- and *cis*-AB-type *meso*-diarylporphyrins **22** and **23** are taken as starting materials instead of *trans-meso*-diarylporphyrins **18** and **19** in Fig. 3.8, porphyrins of additional structural diversity are obtained. Figure 3.11 illustrates synthesis of *cis*-A_2BC-type porphyrin (ZnPBAT) having two *meso*-amino substituents by Imahori and coworkers through Sonogashira coupling, Buchwald–Hartwig double amination, and the second Sonogashira coupling, in sequence starting from 5-mesitylporphyrin **20** (Kurotobi et al. 2013). They investigated on the effect of the asymmetrically enhanced push–pull electronic structure on the DSSC performance and found that introduction of the second amino group caused improvement of the light-harvesting efficiency in visible region and 10% increase in the power conversion efficiency when ZnPBAT was compared with YD2 that is substituted with single diarylamino group

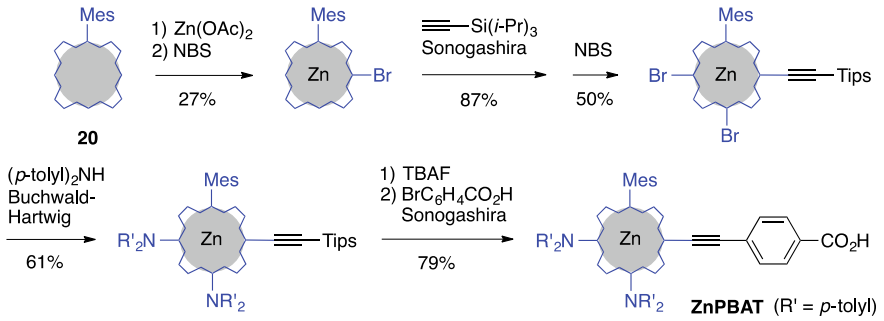

Fig. 3.11 *cis*-A_2BC-type push–pull porphyrin of strong intramolecular dipole moment

at the 5-*meso* position and a 4-carboxyphenylethynyl group at the 15-*meso* position (Table 3.1) (Bessho et al. 2010).

The Grätzel's group reported photosensitizers structurally related to YD2-*o*-C8. Insertion of a 2,1,3-benzothiadiazole unit between the benzoic acid anchoring group and ethyne linker improved PCE performance in the case of GY50 (Yella et al. 2014). Since 2,1,3-benzothiadiazole is strongly electron-withdrawing group, enhanced push–pull effect of GY50 caused red-shift of the absorption bands with more coverage of the visible to NIR wavelength region. Significantly reduced PCE in GY21 indicated that the benzene spacer between the 2,1,3-benzothiadiazole and carboxylic acid plays a key role in suppressing back electron transfer. When the electron-donating effect was strengthened by introducing 2,4-dialkoxyphenyl group at the 5-diarylamino substituent in the case of SM315, 13% PCE was achieved (Mathew et al. 2014). Relationship between photosensitizer structure and PCE is summarized in Table 3.1.

Water-soluble porphyrin, as a photosensitizer, transfers excitation energy to generate singlet molecular oxygen $^1O_2$ that is cytotoxically leading to cell death in photodynamic therapy (PDT) of cancer (Sternberg and Dolphin 1998). Anderson reported A_2BC-type porphyrin **31** that was designed for high intracelluar uptake (Fig. 3.12) (Kuimova et al. 2009). The butadiyne-linked diporphyrin structure of **31** causes conformational change between a planar form and a less stable twisted form through the rotation around the butadiyne axis. The ratio of these conformers was found to depend on the viscosity of the media that was detected by their distinctive fluorescence at 780 nm of the planar form and at 710 nm of the twisted form. The content of the twisted form was found to increase as increase in viscosity, this is because the rotation around the butadiyne axis becomes slower in viscous media. This fluorescent ratiometric molecular rotor provides insight into the diffusion-mediated cellular processes. They found that the diporphyrin **31** incorporated into live cells caused significant increase in the viscosity of the intracellular environment upon irradiation of light. This was interpreted in terms of the crosslinking reactions induced by singlet oxygen generated by the photosensitizing effect of **31**.

Porphyrin-related compounds have been widely studied in the field of PDT due to their intense absorption at long-wavelength visible region that leads to $^1O_2$ generation

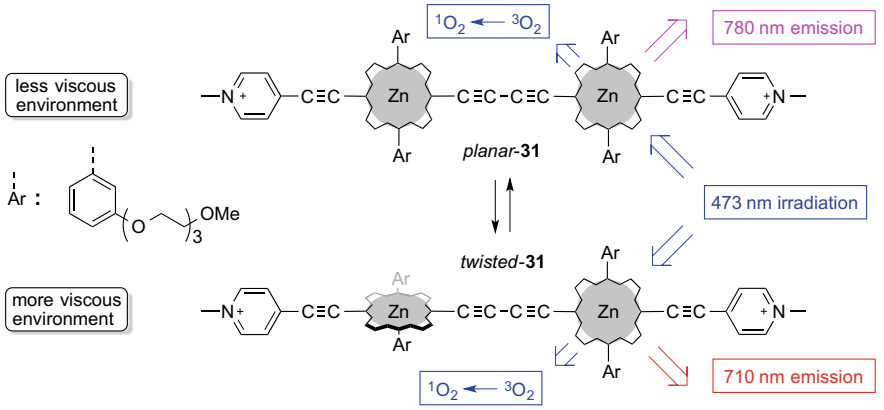

Fig. 3.12 Butadiyne-linked diporphyrin as a fluorescent ratiometric molecular rotor

by way of the triplet excited state due to effective intersystem crossing (Sternberg and Dolphin 1998). Important improvements of the photobiological effect depend on photosensitizers excited by photoirradiation at NIR region (700–1300 nm), because the NIR light can penetrate deeply into the biological tissues. The two-photon absorbing photosensitizers can be photo-excited by intense laser pulses at NIR region and the pinpoint focus of the laser beam enables treatment in the deep area of tissues. Therefore, porphyrin compounds of high two-photon absorption (2PA) efficiency have been extensively studied. The 2PA efficiency is estimated by 2PA cross section (σ) in the unit of GM as the ordinary one-photon absorption depends on the molecular extinction coefficient (ε). Push–pull porphyrin structure with extended π-conjugation is thought to have great magnitude of 2PA cross section as well as in the case of DSSC. Although simple monomeric porphyrins exhibit very small 2PA cross section less than 50 GM with femto-second pulses, the diporphyrin **31** showed a very high 2PA cross section of 17,000 GM with femto-second pulses at 916 nm and its 2PA PDT effect was demonstrated in vivo (Collins et al. 2008).

In the template-directed synthesis of cyclic porphyrin oligomers developed by Anderson and coworkers (Bols and Anderson 2018), 5,15-diarylporphyrin **18** as a starting material was brominated and then subjected to Pd-catalyzed Sonogashira coupling with trialkylsilylacetylene to give 5,15-diaryl-10,20-diethynylporphyrin **32** after desilylation (Fig. 3.13) (Sprafke et al. 2011). In the presence of properly designed template, Glacer oxidative dimerization of the ethyne units was successfully accomplished to give π-conjugated macro ring. The cyclic hexamer of Zn porphyrin *cyclo*-(**32**)$_6$ with butadiyne spacers was formed in 21% yield as a 1:1 complex with hexapyridine template $\mathbf{T}_6$. The fluorescence spectrum of *cyclo*-(**32**)$_6$ •$\mathbf{T}_6$ showed NIR bands ranging from 900 to 1300 nm, and the excited state delocalized over the whole macro ring was generated within less than 0.5 ps after the light absorption.

The dimeric porphyrin **33** worked well in this Glacer homocoupling reaction to afford the same macrocycle in better yield (Fig. 3.14). Although a small amount

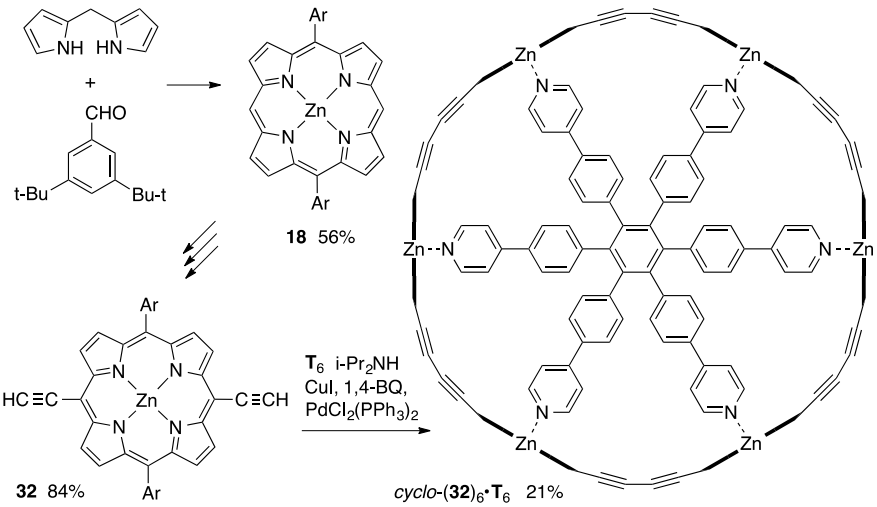

Fig. 3.13 Template-directed synthesis of π-conjugated cyclohexamer of Zn porphyrin

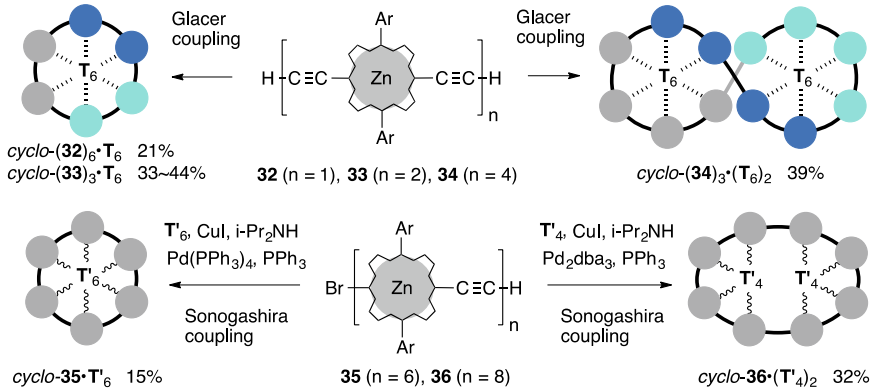

Fig. 3.14 Template-directed synthesis of π-conjugated cyclooligomers of Zn porphyrin

of the cyclododecamer was formed as a byproduct in these cyclization reactions, the Glacer reaction of the butadiyne-linked linear tetramer **34** in the presence of $\mathbf{T}_6$ as a mismatch combination for the *cyclo*-(**32**)$_6$ generated, in 39% yield, a cyclic porphyrin dodecamer *cyclo*-(**34**)$_3$ that includes two template molecules inside the cavity (Kondratuk et al. 2014). A smaller hexapyridine template $\mathbf{T'}_6$ having a hexaethynylbenzene core instead of the hexaphenylbenzene core of the $\mathbf{T}_6$ template was used in the cyclization of ethyne-linked linear oligomers of porphyrin (Rickhaus et al. 2017). The linear ethyne-linked porphyrin hexamer **35** was subjected to Sonogashira coupling reaction to give a 1:1 complex, *cyclo*-**35•T'**$_6$, in 15% yield. A tetrapyridine template $\mathbf{T'}_4$ has a tetraethynylbenzene core and worked well in

the cyclization of the linear ethyne-linked porphyrin octamer **36** by Sonogashira coupling to give a 1:2 complex, *cyclo*-**36**•(**T'**$_4$)$_2$, in 32% yield. The fluorescence band of *cyclo*-**35**•**T'**$_6$ at 1073 nm is red-shifted relative to that of the linear hexamer, *linear*-**35**, at 909 nm and the fluorescence quantum yield of *cyclo*-**35**•**T'**$_6$ is smaller by the factor of 1000, which is indicative of the highly delocalized singlet excited state of the cyclohexamer.

Anderson, Rebane, and coworkers studied two-photon absorption efficiency of their π-conjugated oligomers (Drobizhev et al. 2006). The 2PA cross section values (σ) of the linear Zn porphyrin oligomers increased by 450 times upon going from the monomer **32**(SiR$_3$)$_2$ to the dimer **33**(SiR$_3$)$_2$, but only by 2.4 times from the dimer **33**(SiR$_3$)$_2$ to the tetramer **34**(SiR$_3$)$_2$. The σ value increased gradually from 22,000 GM to 37,000 GM when the porphyrin units increased from 4 to 8 in a series of butadiyne-linked linear oligomers end-capped with trialkylsilyl groups. The 2PA cross section of *cyclo*-(**32**)$_6$ •**T**$_6$ determined by femto-second 2P fluorescence intensity with laser pulses at 1000 nm was 151,000 GM that is much greater than 23,000 GM for the linear hexameric porphyrin oligomer of **32** end-capped with trialkylsilyl groups (Mikhaylov et al. 2016). This great σ value is responsible for the effective π-conjugation over the whole ring that is promoted by the complexation of the template.

3.3 Porphyrins Substituted at Pyrrole β-Positions

3.3.1 Barton–Zard Pyrrole Synthesis

A number of porphyrins with substituents at the pyrrole β-positions are derived from β-substituted pyrroles. Among many synthetic methods for pyrrole ring such as classical Knorr pyrrole synthesis, Barton–Zard synthesis is frequently used because of generality, applicability, and simple procedure. Nitro olefins are generated from nitroaldol products (acetoxynitroalkanes **37**) in situ under basic reaction conditions of Barton–Zard synthesis and then undergo [3+2]-cycloaddition with isocyanoacetate to give 3,4-disubstituted pyrrole-2-carboxylate **38** (Fig. 3.15) (Barton and Zard 1985). The ester function at one of the pyrrole α-positions is regarded as a protecting group, and it can be easily removed or utilized as a *meso*-carbon of porphyrin structure leading to versatile application. A related methodology, van Leusen pyrrole synthesis, using tosylmethyl isocyanide (TosMIC) and Michael acceptor is useful in the synthesis of 3,4-disubstituted pyrroles **39** having electron-withdrawing groups (EWG) at the β-position (van Leusen et al. 1992). 2-Stannylpyrrole **40** was also obtainable in good yields by one-pot procedure, and it is useful in the Stille coupling reactions leading to various building blocks for porphyrin analogues (Dijkstra et al. 1998).

Naturally occurring porphyrins have alkyl substituents at all the pyrrole β-positions. These 2,3,7,8,12,13,17,18-octaalkylporphyrins are different from

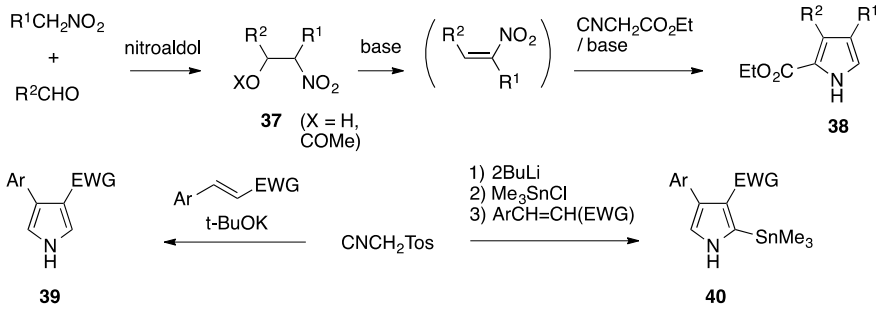

Fig. 3.15 Barton–Zard pyrrole synthesis and van Lausen pyrrole synthesis

5,10,15,20-tetraarylporphyrins in their stereochemistry, electronic structure, and reaction behavior. 2-Carboethoxy-3,4-diethylpyrrole **38** was readily decarboxylated and then subjected to the ordinary porphyrin synthesis using formaldehyde to give octaethylporphyrin (OEP) **41** in 30% yield (Sessler et al. 1992). Ponomarev and coworkers reported that Vilsmeier formylation of OEPCu(II) followed by $NaBH_4$ reduction produced *meso*-(dimethylaminomethyl)OEPCu(II) **42** in good yield. When **42** was allowed to react with MeI, ethylene-bridged diporphyrin **43** was obtained as a bisCu(II) complex (Fig. 3.16) (Borovkov et al. 1999). Binding optically active guest molecule by cooperative metal–ligand coordination bondings forces the bisZn(II) complex to take the face-to-face and skewed orientation of their porphyrin rings. Supramolecular chirogenesis of the bisZn(II) complex was extensively studied in the chirality sensing by Borovkov, Inoue, and coworkers (Borovkov et al. 2004).

Ono, Uno, and coworkers used a Diels–Alder adduct **44** as a nitro olefin equivalent in the Barton–Zard pyrrole synthesis to give ethanoisoindole **45** (Fig. 3.17) (Uno et al. 2000). Phenylsulfenyl chloride addition, MCPBA oxidation, and HCl elimination proceeded in the transformation from **45** to **46**. This reaction sequence is of great importance because simple alkenes are almost quantitatively converted into substrates for Barton–Zard pyrrole synthesis. Diels–Alder adduct **48** between cyclobutadiene and dimethyl acetylenedicarboxylate was also converted to the phenylsulfonyl olefin **49** (Ito et al. 1998, 2001). The phenylsulfonyl olefins **46** and **49** are reactive as well as nitro olefin to give the corresponding pyrroles **47** and **50** in

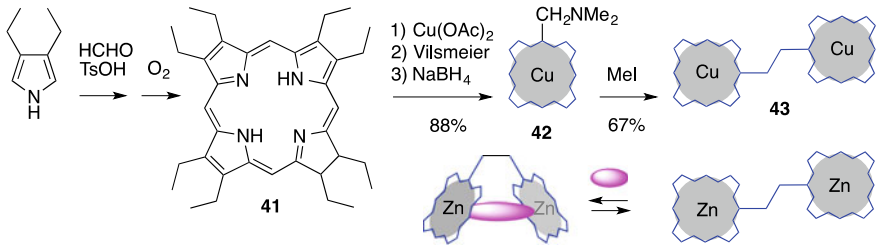

Fig. 3.16 Octaethylporphyrin and ethylene-bridged porphyrin

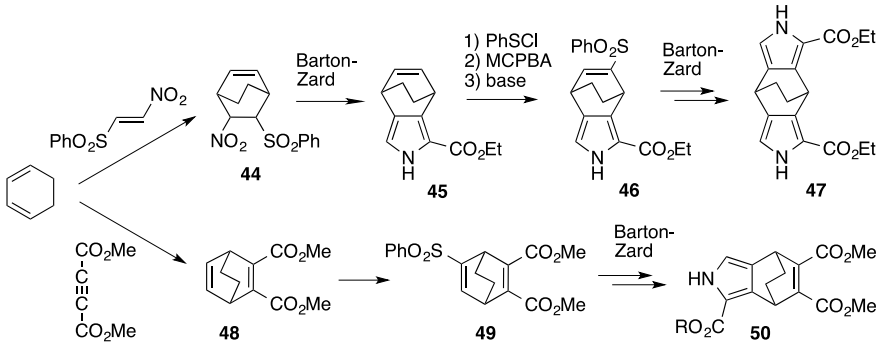

Fig. 3.17 Barton–Zard synthesis of [2,2,2]-octadiene-fused pyrroles

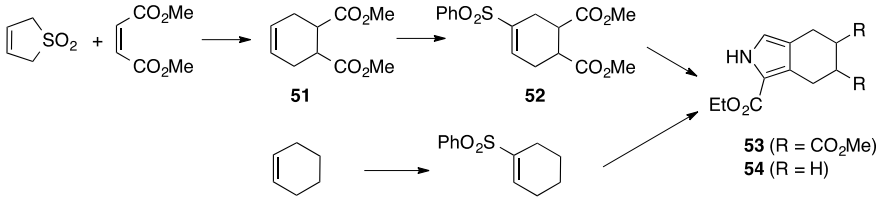

Fig. 3.18 Barton–Zard pyrrole synthesis using cyclohexene

more than 80% yield. These pyrroles were designed to liberate ethylene on pyrolysis by retro Diels–Alder reaction to generate benzo units in the final step of porphyrin synthesis.

Sulfolene as an inexpensive butadiene precursor was conveniently employed by Finikova, Vinogradov, and coworkers in the Diels–Alder reaction to give dicarbomethoxycyclohexene **51**. This Diels–Alder adduct was then converted to phenylsulfonyl cyclohexene **52** and subsequently to the tetrahydroisoindole **53** by Barton–Zard reactions (Finikova et al. 2001). When cyclohexene was taken as a starting material, the α-free pyrrole **54** was also obtained in good yield (Fig. 3.18) (Finikova et al. 2004). These cyclohexene-fused pyrrole units are readily converted into the benzene-fused pyrrole units by oxidation under mild reaction conditions especially after porphyrin ring formation.

3.3.2 Benzoporphyrins

Tetrabenzoporphyrins where benzene rings are fused at the pyrrole β-positions are chemically stable, and their extended π-conjugation stabilizes their cationic states, which changes the basicity and redox potentials. In addition to these features, the

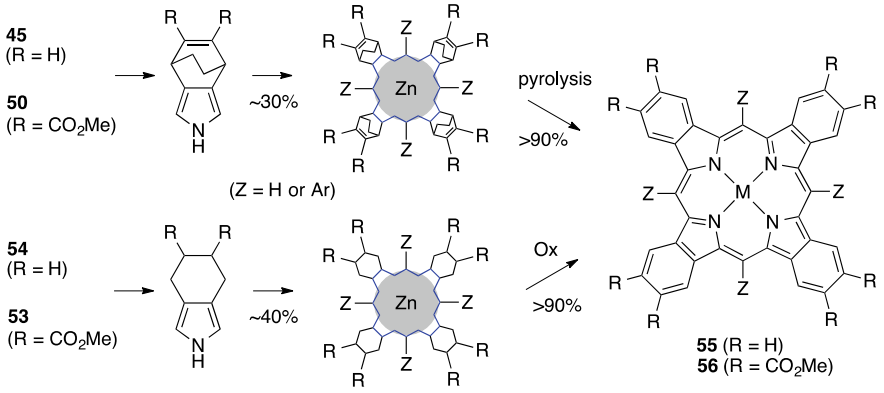

Fig. 3.19 Synthesis of benzoporphyrins

red-shifted UV–vis absorption spectra of benzoporphyrins are suitable as optoelectronic materials. The above-mentioned pyrroles **45**, **50**, **53**, and **54** are important building blocks for benzoporphyrins. Since the highly planar benzoporphyrins tend to form a face-to-face stacked array leading to insoluble materials, purification is usually difficult. The precursor porphyrins substituted with aliphatic groups at the pyrrole β-positions were prepared in 30–40% yield from the corresponding pyrroles by condensation with formaldehyde and aryl aldehydes. These porphyrins can be dissolved in organic solvents and circumvent problems associated with low solubility of benzoporphyrins (Fig. 3.19) (Carvalho et al. 2013). High temperature at ~200 °C is needed to induce retro Diels–Alder reaction in the pyrolysis as the final step to tetrabenzoporphyrins **55** and **56** starting from **45** and **50** (Ito et al. 1998, 2001). These porphyrins were alternatively obtained in good yields under much milder reaction conditions by oxidative aromatization starting from **53** and **54**, but oxidizing agents like metal salt, DDQ, or acid are needed (Finikova et al. 2001, 2004). The retro Diels–Alder method allows preparation of device assemblies of benzoporphyrins by introducing precursor porphyrins into the device assemblies before pyrolysis.

In the UV–vis spectrum of *meso*-unsubstituted benzoporphyrin **56** (Z = H), the Soret band at 454 nm and the Q band at 648 nm are red-shifted by 49 nm and 84 nm, respectively, relative to the bicyclo[2.2.2]octadiene-fused precursor (Table 3.2). In particular, this Q band of **56** (Z = H) is very strong with its absorption coefficient being in the order of 10^5 M^{-1} cm^{-1} (Ito et al. 2001). UV–vis absorption bands of *meso*-tetraphenylbenzoporphyrin **56** (Z = Ph) are further red-shifted by ~30 nm relative to **56** (Z = H).

Uno and coworkers prepared bicyclo[2.2.2]octadiene-fused dimeric porphyrin **57** in 21% yield using double 3+1 condensation of tripyrrane and the dipyrrole derived from **47** (Fig. 3.20). Subsequent retro Diels–Alder reaction afforded benzene-fused dimeric porphyrin **58** (Uno et al. 2007). The strong Soret band of **58** (M = 2Zn) at 475 nm is significantly red-shifted from those (399 nm and 414 nm) of **57** (M = 2Zn) (Table 3.2). The Q band of **58** at 638 nm is as intense as the Soret band and

Table 3.2 Selected major UV–vis absorption bands of benzoporphyrins

Porphyrin	λ_{max} nm (log ε)		solvent
	Soret bands	Q bands	
55 (M = Zn, Z = Ph)	463 (6.44)	609 (5.09), 652 (5.68)	$CHCl_3$
56 (M = Zn, Z = Ph)	485 (5.65)	621 (4.35), 667 (4.85)	$CHCl_3$
56 (M = Zn, Z = H)	454 (5.62)	597 (4.28), 648 (5.06)	$CHCl_3$
57 (M = 2Zn)	399 (5.65), 414 (5.65)	533 (4.40), 574 (4.74)	$CHCl_3$
58 (M = 2Zn)	394 (4.98), 475 (5.36)	621 (4.78), 638 (5.32)	C_5H_5N
60 (M = 5Zn)	404 (5.82), 423 (5.61)	534 (4.83), 573 (4.90)	$CHCl_3$
61 (M = 5Zn)	415 (5.56), 498 (5.32)	721 (4.80), 763 (5.61)	C_5H_5N

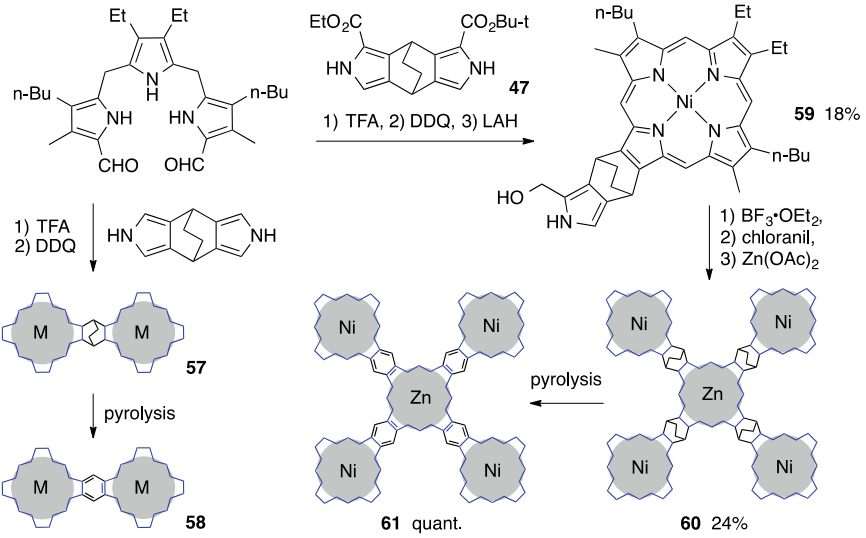

Fig. 3.20 Benzene-fused multiporphyrins

red-shifted by 64 nm in comparison with weak Q bands of **57** at 533 nm, and 574 nm. The single 3+1 condensation of tripyrrane and dipyrrole **47** followed by reduction of the ester group gave bicyclo[2.2.2]octadiene-fused porphyrin **59** in 18% yield. The pyrrole-2-carbinol part of **59** reacted under ordinary reaction conditions of porphyrin synthesis to give 24% yield of the pentameric porphyrin **60** where four porphyrin rings are connected to the pyrrole β-positions of the central porphyrin ring. Pyrolysis

of **60** proceeded almost quantitatively to generate cruciform porphyrin **61** that has overall π-conjugation among 5 porphyrin units (Uoyama et al. 2010).

The UV–vis spectrum of **61** (M = 5Zn) showed strong Soret bands at 415 nm and 498 nm. These Soret bands are red-shifted from those (404 nm and 423 nm) of **60** (M = 5Zn) (Table 3.2). The Q band of **61** (M = 5Zn) at 763 nm is as intense as the Soret band and far red-shifted in comparison with weak Q bands of **60** (M = 5Zn) at 534 nm, and 573 nm and also with the Q band (638 nm) of the benzene-fused dimeric Zn porphyrin **58** (M = 2Zn), whereas the UV–vis spectra of bicyclo[2.2.2]octadiene-fused oligomeric Zn porphyrins **57** and **60** are not so different from that of monomeric Zn porphyrin.

Two-photon absorption cross section provides information on how far the π-conjugation is expanding in the molecular systems. The 2PA cross section values of the benzene-fused oligomeric Zn porphyrin **58** (M = 2Zn) and **61** (M = 5Zn) measured by z-scan method were reported as 3000 GM (λ_{ex} 1275 nm) and 3900 GM (λ_{ex} 1500 nm), respectively (Uoyama et al. 2010). These values are much larger than those (<100 GM) of monomeric porphyrins, but they are less than those (10^4–10^5 GM) of *meso,meso*-butadiyne-linked multiporphyrins like **33**$(SiR_3)_2$ and **34**$(SiR_3)_2$. It was suggested that electronic interaction between porphyrin π-systems by way of the pyrrole β-positions is not so effective as by way of the *meso*-positions.

Smith and coworkers prepared the cruciform porphyrin having four *meso*-tetraphenylporphyrin units instead of *meso*-unsubstituted porphyrin units of **61** in a simple procedure (Jaquinod et al. 1998). The phenylsulfonyl group was introduced into sulfolene itself through phenylsulfenyl chloride addition, MCPBA oxidation, and HCl elimination and then subjected to the Barton–Zard pyrrole synthesis. Pyrolysis of the resulting sulfolene-fused pyrrole **62** at 240 °C in the presence of *meso*-tetraphenylporphyrin (TPP) produced pyrroloporphyrin **64** in ca. 30% yield after DDQ oxidation of the initially formed pyrrolochlorin **63** (Fig. 3.21). The pyrroloporphyrin **64** was reduced to the corresponding carbinol that is an analogue of **59** and then converted into the cruciform porphyrin after DDQ oxidation.

Smith and coworkers also used *meso*-tetraphenylporphyrin (TPP) as a starting material in the synthesis of directly β-fused porphyrin trimer **66** (Fig. 3.22) (Paolesse et al. 2000). Readily available mononitroTPPNi(II) was regarded as a substrate for the Barton–Zard synthesis and it actually gave pyrroloporphyrin **65** after decarboxylation. It is noteworthy that β-nitroporphyrins react in a similar

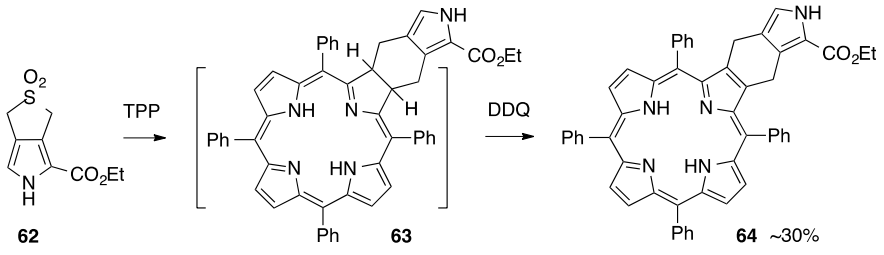

Fig. 3.21 TPP-derived building block of cruciform porphyrin

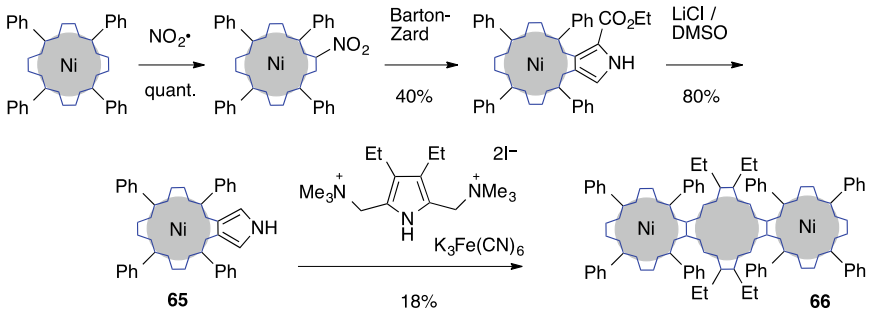

Fig. 3.22 Directly linked trimeric porphyrin

fashion to nitroalkene. Bisquarternary ammonium salt derived from 2,5-bis(N,N-dimethylaminomethyl)pyrrole was allowed to react with **65** under neutral conditions in the presence of oxidizing agent to afford 18% yield of the target porphyrin **66**. This β-fused trimer showed intense UV–vis bands at 486 nm (log $\varepsilon = 5.3$) and 716 nm (log $\varepsilon = 5.2$).

Kräutler and coworkers obtained sulfolene-fused porphyrin **67** in 44% yield by ordinary condensation reaction of arylaldehyde and solfolene-fused pyrrole that is derived from **62** (Fig. 3.23). Pyrolysis of **67** at 140 °C in the presence of 1,4-benzoquinone induced [4+2] cycloaddition and subsequent DDQ oxidation and metal insertion generated tetrabenzoporphyrin **68** with further π-conjugation to the quinone moieties (Banala et al. 2009). Fusion of 1,4-naphthoquinone instead of benzene at the pyrrole β-positions of *meso*-tetraarylporphyrin caused red-shifts of the Soret band by ~90 nm and of the Q band by ~70 nm in their UV–vis spectra (the major absorptions at 555 nm and 725 nm) of **68** in chlorinated solvents. **68** is a black-colored porphyrin with the lowest absorption coefficient (8700 M^{-1} cm^{-1}) over the whole UV–vis range (230–770 nm) seen as an absorption valley at 634 nm.

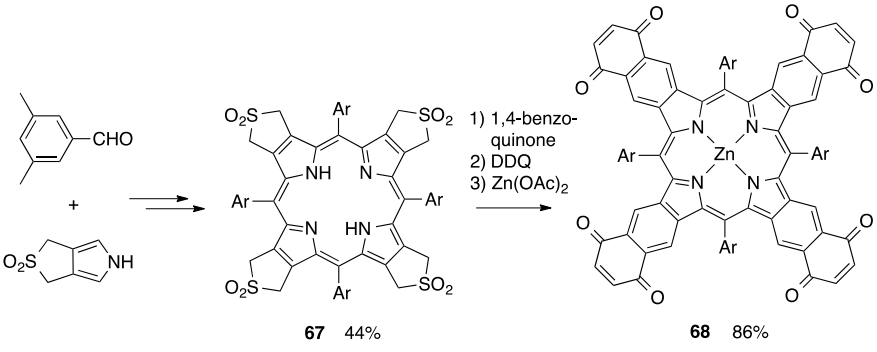

Fig. 3.23 A black-colored 1,4-naphthoquinone-fused porphyrin

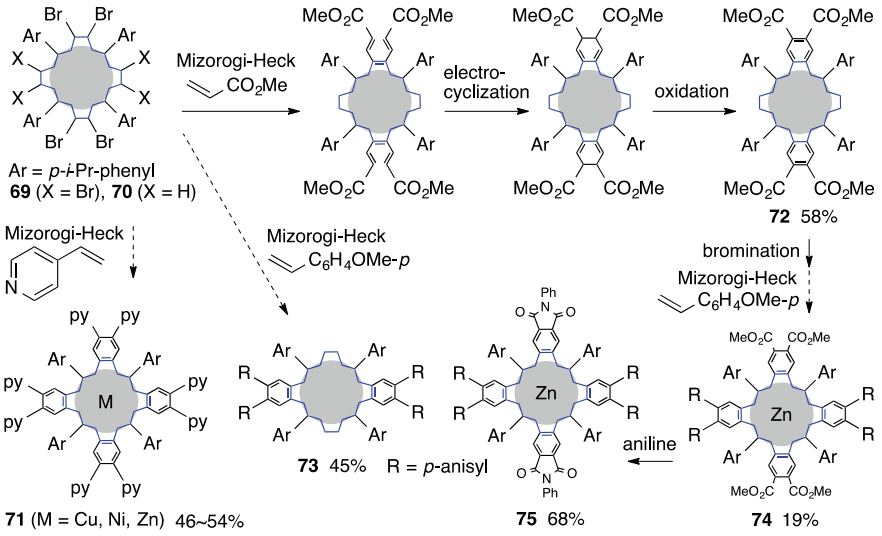

Fig. 3.24 Water-soluble porphyrin and push–pull porphyrin

Organometallic synthetic methods were applied in synthesizing benzoporhyrins by way of brominated *meso*-tetraarylporphyrins **69** and **70** that were obtained by using N-bromosuccinimide (NBS). Tetrabromination occurs regioselectively at the opposite pyrrole rings of the *meso*-tetraarylporphyrin free base in ~60% yield and octabromination of the Ni complexes proceeds in more than 80% yield (Chumakov et al. 2009). Water-soluble porphyrins are useful especially in the biomedical application, and *meso*-tetraarylporphyrins where four *meso*-aryl groups are pyridinium or aryl sulfonate have been frequently studied. Highly water-soluble porphyrins with eight hydrophilic groups at all the pyrrole β-positions have been synthesized recently through one-pot three-step reactions of Cu, Ni, and Zn complexes of **69** and vinylpyridines using Pd catalyst in 46–54% yields (Fig. 3.24) (Jiang et al. 2012). These metal complexes of *meso*-tetraaryltetrabenzoporphyrin **71** (M = Zn) can be protonated at the eight pyridyl units, which caused red-shifts by ~30 nm of the Soret band to 525 nm and the Q band to 708 nm. The Q band at 684 nm of the protonated complex of **71** (M = Ni) showed unusually high intensity as a monomeric metalloporphyrin. This octacation of **71** could be dissolved in distilled water with concentration more than 15 mM. When the tetrabromoporphyrin **70** was allowed to react with methyl acrylate under similar reaction conditions, the one-pot reactions of Mizorogi-Heck coupling, 6π-electrocyclization, and oxidative aromatization occurred to give the dibenzoporphyrin **72** with four methyl ester units in 58% yield. **72** was converted into the Zn(II) tetrabromodibenzoporphyrin in 42% yield and then subjected to the Pd-catalyzed coupling reaction with 4-methoxystyrene under the same Mizorogi-Heck conditions. The Zn(II) tetrabenzoporphyrin **74** formed in

45% yield was further converted to the push–pull porphyrin **75** with two benzenedicarboximide units as electron-withdrawing groups and two 3,4-di-*p*-anisylbenzene units as electron-donating groups (Kumar et al. 2018).

The push–pull tetrabenzoporphyrin Zn complex **75** showed the Soret absorption band at 507 nm that is red-shifted by 51 nm in comparison with the dibenzoporphyrin Zn complex of **73** with two 3,4-di-*p*-anisylbenzo units. It is also red-shifted by 30 nm in comparison with the dibenzoporphyrin Zn complex with two benzenedicarboximide unit derived from **72**. The Q band of **75** at 721 nm appeared at by ca. 80 nm longer wavelength than those push-only or pull-only dibenzoporphyrins. Theoretical study on the electronic structure indicated that the HOMO–LUMO gaps of the push-only and pull-only dibenzoporphyrins are not so different although both HOMO and LUMO energy levels of the push-only dibenzoporphyrin are higher than those of the pull-only dibenzoporphyrin. It is of interest that the HOMO energy level of **75** is very similar to that of the push-only dibenzoporphyrin and the LUMO energy level of **75** is very similar to that of the pull-only dibenzoporphyrin, which significantly reduced the HOMO–LUMO gap. This result was consistent with the cyclic voltammetric analysis; 1.75 V for **75** is by 0.25 V smaller than those dibenzoporphyrins.

3.3.3 Reactions of Porphyrins at Pyrrole β-Positions

Since *meso*-tetraarylporphyrins are readily available, robust, and soluble in organic solvents, great effort has so far been directed to structural modification at pyrrole β-positions. Bringmann and coworkers investigated Pd-catalyzed borylation of 2-bromo-*meso*-tetraphenylporphyrin **76** and obtained β-dioxaborolanylporphyrin **77** in 70% yield using toluene–water two phase system (Fig. 3.25) (Bringmann et al. 2008). If this reaction was run in DMF, carbopalladation on the adjacent *meso*-phenyl group occurred to give almost exclusive formation of indene-fused porphyrin **78** without participation of bis(pinacolato)diboron ($B_2(pin)_2$) in the reaction. A closely related cyclopentadiene-fused porphyrins **80** was reported by Osuka's group through Pd-catalyzed reaction between *meso*-bromoporphyrin **79** and alkynes (Sahoo et al. 2006). The Ni and Cu complexes **80** showed split Soret bands; one at 380–390 nm and the other at 480–490 nm. The additional π-conjugation in **80** (M = Ni) decreased electrochemical HOMO–LUMO gap ($\Delta E = 1.66$ V) relative to that ($\Delta E = 2.29$ V) of *trans*-A_2 type diarylporphyrin Ni complex. Once β-borylated porphyrin **77** was available, it was subjected to the Pd-catalyzed Suzuki–Miyaura cross coupling with **76** leading to β,β-linked diporphyrin **81** in 73% yield. Some bimetallic complexes of **81** could be resolved into enantiomers by HPLC on a chiral phase. The rotational stability at the β,β-axis depends on the metal but racemization of the optically resolved bisZn complex was not seen at room temperature.

Osuka, Shinokubo, and coworkers reported that the pyrrole β-position adjacent to the unsubstituted *meso*-position could be directly borylated (Hata et al. 2005). When the $[Ir(COD)OMe]_2$-catalyzed direct borylation of aromatic compounds by $B_2(pin)_2$ was applied to 5,15-diarylporphyrin and 5,10,15-triarylporphyrin, the

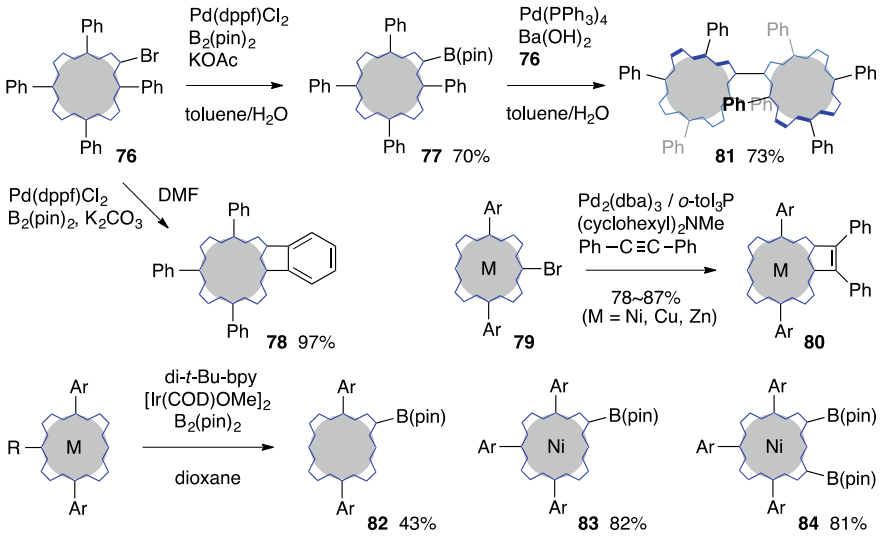

Fig. 3.25 Borylation of porphyrins

3,3,4,4-tetramethyldioxaborolanyl group was introduced selectively through the C-H activation at the pyrrole β-position that is sterically less congested than the *meso*-position. By changing the $B_2(pin)_2$/porphyrin ratio, monoborylated and diborylated porphyrins (**82**, **83**, **84**) were obtained in 43–82% yield. These borylated porphyrins were conveniently employed for various Pd-catalyzed cross-coupling reactions.

The pyrrole β-position of *meso*-tetraarylporphyrins is functionalized by oxidation reactions (Fukui et al. 2017). Brückner, Rettig, and Dolphin reported that OsO_4-mediated *cis*-dihydroxylation of $TPPH_2$ and TPPNi(II) gave 2,3-dihydroxy-*meso*-tetraarylchlorin **87** in 49% and 72% yield, respectively (Fig. 3.26) (Brückner et al. 1998). These compounds were further oxidized by DDQ to generate 2,3-dioxochlorins **88** in 73 and 65% yield (Daniell et al. 2003). **88** was alternatively synthesized by Crossley and coworkers by oxidizing β-amino- and β-hydroxyporphyrin **85** and **86** that were prepared conveniently from β-nitroporphyrin (Crossley and King 1984; Crossley et al. 1991). The Crossley's group utilized this 2,3-dioxochlorin **88** as a key compound in the development of various porphyrin oligomers of extended π-conjugation. The dimeric porphyrin **90** (n = 0) that was prepared by condensation of **88** with 1,2,4,5-tetraaminobenzene was converted to the 12,12′,13,13′-tetraoxobischlorin and then reacted with 1,2,4,5-tetraaminobenzene and **88** at both ends. Thus formed tetrameric porphyrin **90** (n = 2) showed electrochemical HOMO–LUMO gap of 0.8 eV (Crossley and Burn 1991). Brückner and coworkers obtained a pyrrole-modified porphyrin called indaphyrin **91** from 2,3-dihydroxy-*meso*-tetraarylchlorin **87** under acidic aerobic conditions (McCarthy et al. 2004). That is, a secochlorin bisaldehyde intermediate formed by the oxidative

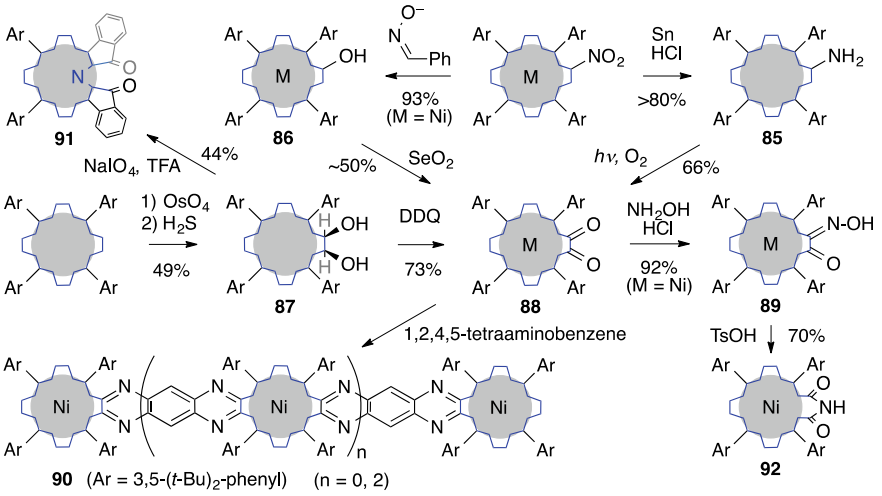

Fig. 3.26 Oxidative functionalization at the pyrrole β-position

C–C bond cleavage of the vicinal diol part of **87** with sodium periodate undergoes Friedel–Crafts type aromatic substitution at the *meso*-phenyl *ortho*-position promoted by trifluoroacetic acid (TFA).

Indaphyrin **91** and its metal complexes have a helical conformation in order to relieve electronic repulsion of carbonyl oxygens to one another and each resolved enantiomer was quite stable with a racemization barrier greater than 113 kJ/mol at 25 °C. UV–Vis spectrum of **91** and its metal complexes show broad absorptions in the region between 400 and 600 nm. Free base **91** has split Soret-like bands at 419 nm and 554 nm with $\varepsilon = \sim 4 \times 10^4$ (Samankumara et al. 2015; Götz et al. 2015). α-Keto oximes **89** formed from metal complexes **88** (M = Ni, Pd, Pt) of 2,3-dioxochlorins readily underwent Beckmann rearrangement with *p*-toluenesulfonic acid (TsOH), in which case the pyrrole-3-oxo-4-oxime part was converted into 6-membered pyrazine imide in the product **92** (Akhigbe and Brückner 2013).

3.4 π-Extended Porphyrins

3.4.1 Electrophilic Substitution with meso*-Aryl Groups*

π-Extension of porphyrin core causes great influence on the absorption bands and redox potentials, which extends the applicability of porphyrin compounds to various scientific fields. Porphyrins with *meso*-acetylene groups (appeared in 3.1.4), benzoporphyrin derivatives (appeared in 3.2.2), and linear oligomers **66** and **90** are examples of this category. π-Conjugation between *meso*-aryl groups and porphyrin core

could be enabled by simple procedure as already mentioned in the compounds **78**, **80**, and **91**.

Callot and coworkers used Friedel–Crafts acylation as a key reaction in connecting *meso*-aryl *ortho*-positions and pyrrole β-positions (Fig. 3.27) (Richeter et al. 2003). *cis*-A_2B_2 type *meso*-tetraarylporphyrin **93** was obtained in 5.1% yield from the porphyrin products mixture in the mixed condensation of pyrrole, *o*-methoxycarbonylbenzaldehyde, and 3,5-di-*t*-butylbenzaldehyde in the ratio of 2:1:1. The ester group of **93** was converted into acid chloride and then subjected to Friedel–Crafts reaction conditions. The major product **94** obtained in 44% had bistetralone-fused porphyrin structure. The Soret band at 516 nm (log $\varepsilon = 4.9$) and the Q band at 738 nm (log $\varepsilon = 4.1$), 826 nm (log $\varepsilon = 4.1$) in the UV–vis spectrum were remarkably red-shifted. A mixture of 2,12- and 2,13-dibromoTPPH$_2$ **95** obtained by regioselective dibromination of TPPH$_2$ was reacted with CuCN to give di-cyanoTPPCu **96** effectively by nucleophilic aromatic substitution. Hydrolysis of the cyano group followed by a similar Friedel–Crafts procedure afforded differently bistetralone-fused porphyrins **97** and **98** in 27% and 30% yield, respectively, after chromatographic separation.

Brückner's group also showed that if α-keto oxime free base **89** was reacted with TsOH, the Beckmann rearrangement leading to **92** was suppressed and the adjacent *meso*-phenyl group participated to generate a quinoline ring leading to mono- and bisquinoline-fused porphyrins **100** and **103** (Fig. 3.28) (Akhigbe et al. 2015). These pyrrole-modified porphyrins were alternatively synthesized in better yields through DDQ oxidation of the oxime moiety of **89** and **100** by way of mono- and bisquinoline N-oxide **99** and **101**. These quinoline-fused porphyrin free bases show Q bands in the range of 730–780 nm. Ruppert and coworkers reported that the bisquinoline-fused

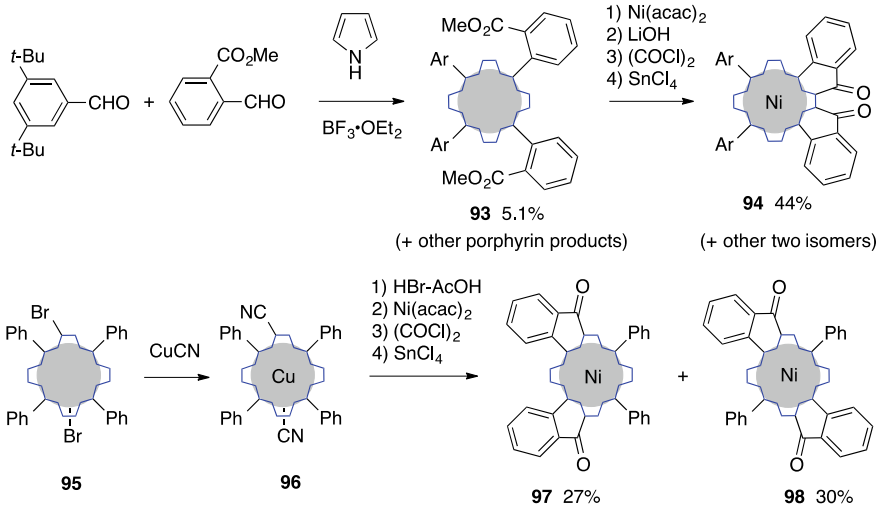

Fig. 3.27 Friedel–Crafts acylation between the *meso*-aryl *o*-position and the pyrrole β-position

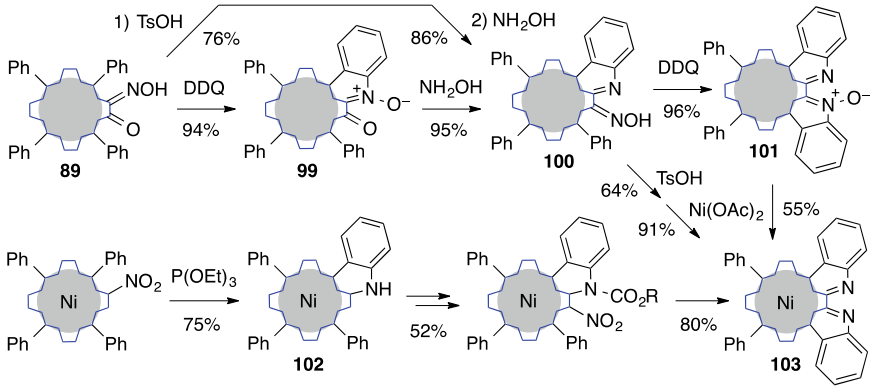

Fig. 3.28 Pyrrole-modified porphyrins with quinoline-fusion

porphyrin **103** was regarded to have an external bidentate coordination site and can be obtained in a shorter synthetic route starting from readily available β-nitroporphyrin (Jeandon and Ruppert 2011). *meso*-Phenyl C-H insertion of nitrene generated from nitro group with triethyl phosphite afforded dihydroquinoline-fused porphyrin **102** effectively. Protection of the NH group and nitration of **102** followed by just heating produced **103** in good yield.

3.4.2 Oxidative Coupling of β-Aminoporphyrins

β-Aminoporphyrins were readily prepared and showed interesting reactions that are owing to their nature of being easily oxidized. β-Amino-*meso*-tetraarylporphyrins **85** were conveniently applied to synthesizing dimeric porphyrins (Fig. 3.29). Bringmann and coworkers intended to obtain β,β-linked diporphyrin **104** by Ullmann coupling of 2-amino-3-bromoporphyrin **105**, but the product obtained in 78% yield turned out to be pyrazine-fused diporphyrin (M = Ni) **106** (Bruhn et al. 2014). The β,β-linked diporphyrin **104** was formed from **85** (M = Ni) in 94% yield by oxidizing with $AgPF_6$. **104** is intrinsically chiral diporphyrin, and its conformational change by rotation around the β,β-axis is inhibited even at 100 °C. In comparison with the bisNi complex of diporphyrin **81**, stereochemical stability is significantly increased by the presence of amino groups. The pyrazine-fused diporphyrin **106** (M = Zn) was also synthesized by Mandoj, Paolesse, and coworkers by reacting 2,3-diamino-*meso*-tetraphenylporphyrin **107** with 2,3-dioxochlorin **88** or diethyl oxalate (Mandoj et al. 2013). Shinokubo and coworkers recently investigated DDQ oxidation of β-aminoporphyrins **85** (M = Ni) with bulky *meso*-tetraaryl groups and found formation of the pyrazine-fused diporphyrin **108** in high yields (Ito et al. 2015). Although *meso*-tetraphenyl derivatives **106** take C_{2h} symmetric conformation, *meso*-tetramesityl derivative **108** has twisted π-conjugation system of D_2 symmetry. The

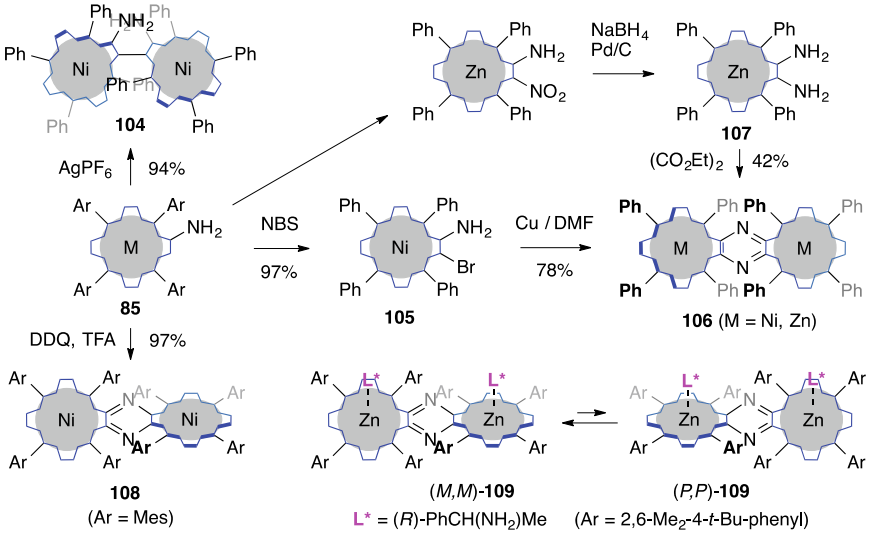

Fig. 3.29 Oxidative dimerization of aminoporphyrins

bisZn complex **109** is interchanging rapidly between a (*M, M*)-form and a (*P, P*)-form and binding (*R*)-1-phenylethylamine induced helical sense bias in favor of the (*M, M*)-form with 65:35 diastereoselectivity (Ito et al. 2016).

Fujimoto and Osuka demonstrated that π-conjugation between two porphyrin cores is much more enhanced by 1,5-naphthyridine-fusion in comparison with the pyrazine-fusion seen in **106** (Fujimoto and Osuka 2018). The 1,5-naphthyridine-fused diporphyrin **112** was obtained in 84% yield by Pt(II)-catalyzed cyclization of bisNi(II) complex of β-to-β ethynylene-bridged *meso*-aminoporphyrin dimer **111** followed by oxidation with PbO_2 (Fig. 3.30). Ni(II) complex **111** was prepared starting from β-borylporphyrin **83** by NIS-CuI iodination, (Fujimoto et al. 2014)

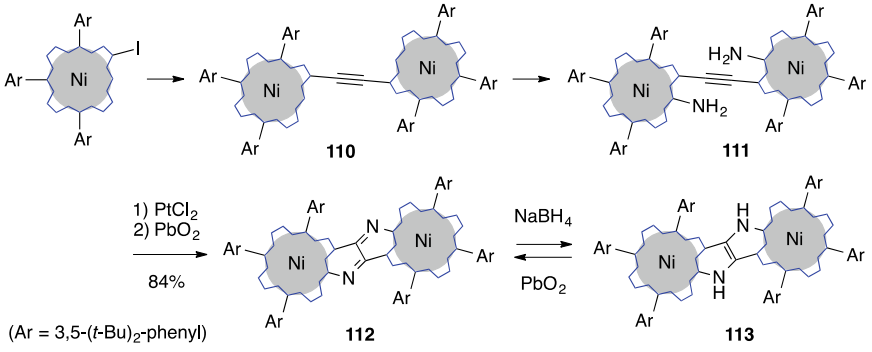

Fig. 3.30 1,5-Naphthyridine-fused diporphyrin

Table 3.3 UV–vis and near-infrared absorption bands of π-extended porphyrins and their electrochemical HOMO–LUMO gap

Porphyrin	λ_{max} nm (log ε)		Electrochemical HOMO–LUMO gap (V)
	Soret band	Q band	
106 (M = 2Ni)	480 (5.0)	619 (4.1)	2.16
112 (M = 2Ni)	521 (5.1)	1011 (5.0)	0.99
115 (free base)	474 (5.30)	698 (4.82)	1.66
117 (M = Ni)	648 (4.8)	1136 (4.7)	1.01
119 (M = Ni)	842 (4.85)	1417 (5.07)	0.61
121 (M = 2Zn)	590 (5.19)	1141 (4.71)	1.09
122 (M = 2Zn)	618 (5.24)	1323 (5.05)	0.84
124 (M = 2Zn)	657 (5.05)	1322 (5.16)	0.62
126 (M = 2Zn)	665 (5.26)	1495 (5.16)	0.77

Sonogashira coupling, nitration with $AgNO_2$-I_2, and reduction with $NaBH_4$-Pd/C. The UV–vis major band of **106** (M = Zn) appears at 492 nm (log ε = 5.06) and their Q bands are at shorter wavelength region than 650 nm. Its electrochemical HOMO–LUMO gap is 2.16 V that is only slightly smaller than 2.24 V of TPPZn. In contrast, the HOMO–LUMO gap (0.99 V) of **112** measured by cyclic voltammetry is remarkably smaller than the reduced form **113** (1.8 V). The major absorption bands of **112** at 521 nm (log ε = 5.1) and 1011 nm (log ε = 5.0) are far red-shifted in comparison with those (496 and 663 nm) of **113** (Table 3.3).

3.4.3 Oxidative Fusion of Porphyrin Periphery

Oxidative coupling of aromatic rings with dehydrogenative C–C bond formation is a versatile method for extending π-conjugation (Grzybowski et al. 2013). This Scholl type oxidation has been applied to porphyrin compounds (Lewtaka and Gryko 2012). Stepien and coworkers introduced phenanthrene units at the periphery of porphyrin using Scholl type oxidation (Fig. 3.31) (Mysłiwiec et al. 2012). 3,4-Diarylpyrrole that was prepared by Barton–Zard reaction was converted to octakis(3,4-dialkoxyphenyl)porphyrin **114** in 62% yield. Scholl oxidation of the Zn complex of **114** with $FeCl_3$ proceeded to give 97% yield of the tetraphenanthroporphyrin **115**. This efficient transformation to highly π-extended porphyrin **115** is noteworthy. The π-extension caused red-shift of the Soret band from 427 to 474 nm, and the maximum Q band intensity increased from 4.38 (log ε at 522 nm) to 4.90 (log ε at 650 nm). The electrochemical HOMO–LUMO gap decreased from 2.27 to 1.66 V upon going from **114** to **115**.

More effective π-extension is enabled by oxidative aromatic coupling between *meso*-aryl groups and porphyrin core (Fig. 3.32). Osuka and coworkers obtained

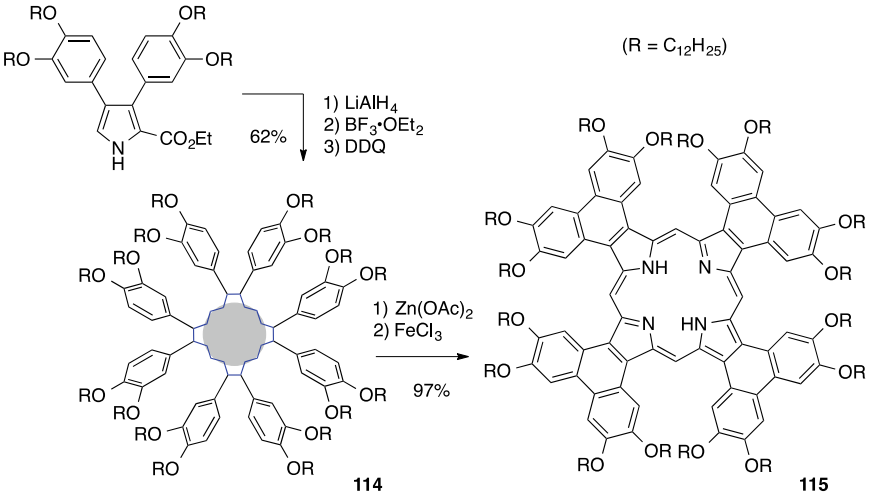

Fig. 3.31 Scholl oxidation to tetraphenanthroporphyrin

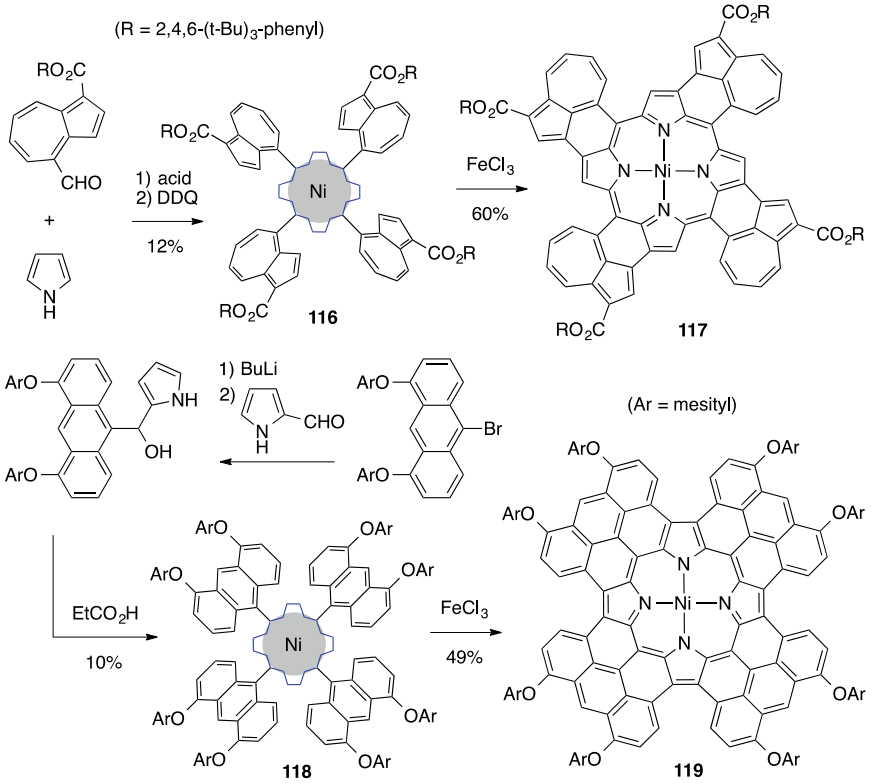

Fig. 3.32 Quadruply azulene- and anthracene-fused porphyrins

Ni(II) *meso*-tetraazulenylporphyrin **116** and then it was successfully converted to the fully azulene-fused porphyrin **117** by $FeCl_3$-mediated oxidation. The special ester substituents (2,4,6-tri-*t*-butylphenyl ester) allowed clean oxidation in 60% yield (Kurotobi et al. 2006). The Ni complex **117** showed strong absorption bands at 684 nm (log $\varepsilon = 4.8$) and 1136 nm (log $\varepsilon = 4.7$) (Table 3.3). This significantly red-shifted spectrum, and the well diminished electrochemical HOMO–LUMO gap (1.01 V) illustrate the great effect of azulene fusion. The 2PA cross section value ($\sigma = 7170$ GM) of **117** measured at 1380 nm excitation was very high as a monomeric porphyrin (Pawlicki et al. 2009). The quadruply fused Ni porphyrin **119** was also prepared by Anderson and coworkers (Davis et al. 2011). The eightfold oxidative ring closure occurred at the pyrrole-β-positions of Ni(II) *meso*-tetra-9-anthracenylporphyrin **118** that was prepared by condensation of 9-anthracenyl-2-pyrrylmethanol. It is remarkable that the Q band of **119** appeared at extremely long wavelength (1417 nm) with a remarkable intensity (log $\varepsilon = 5.07$) that is greater than the Soret-like absorption at 842 nm (log $\varepsilon = 4.85$) (Table 3.3). The electrochemical HOMO–LUMO gap of 0.61 V was very small.

Scholl type oxidation was applied to introduce direct triple bridges between two porphyrin cores of *meso*-triarylporphyrins (Fig. 3.33). Thompson and coworkers oxidized 5,15-diaryl-10-pyrenylporphyrin Zn(II) complex **120** with DDQ-$Sc(OTf)_3$ to give *β,β*-, *meso,meso*-, *β',β'*-triply fused diporphyrin **121** (Diev et al. 2010). This diporphyrin was further oxidized with $FeCl_3$ to cause oxidative coupling between *meso*-pyrenyl groups and pyrrole β-positions. The fully fused Zn complex **122** showed the major absorptions at 618 nm (log $\varepsilon = 5.24$) and 1323 nm (log $\varepsilon =$

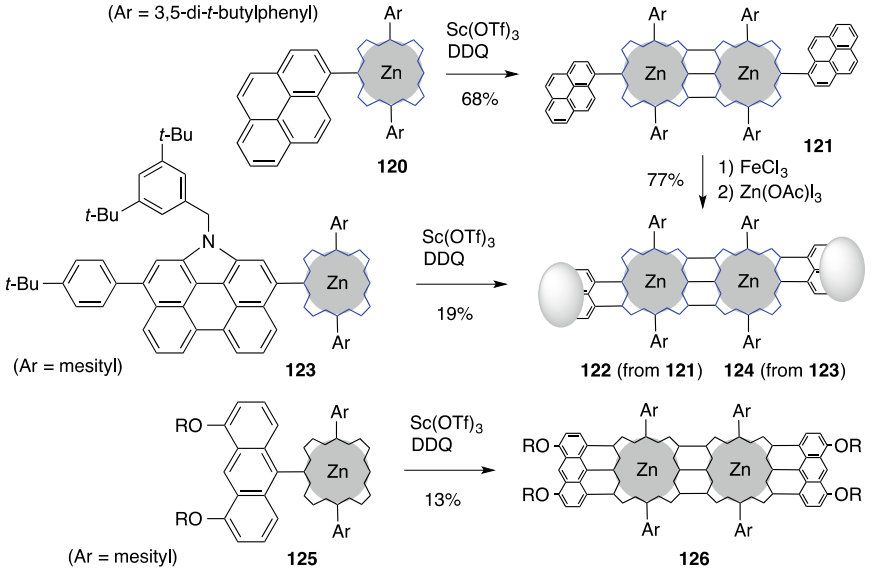

Fig. 3.33 *β,β*-, *meso,meso*-, *β',β'*-triply fused porphyrin dimers

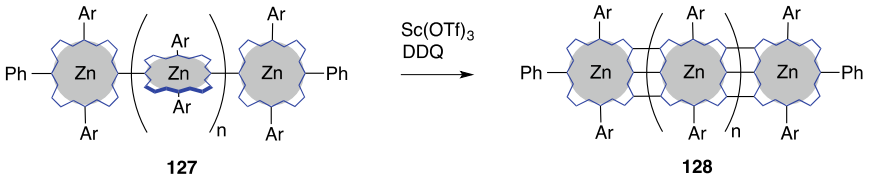

Fig. 3.34 *β,β-*, *meso,meso-*, *β',β'*-triply fused porphyrin dimers

5.05). This NIR band of **122** is red-shifted by 182 nm and the electrochemical HOMO–LUMO gap (0.84 V) of **122** decreased by 0.25 V in comparison with those of **121** (Table 3.3). Kim and coworkers studied this oxidation chemistry of *meso*-triarylporphyrin **123** having a N-annulated perylene group instead of a pyrenyl group of **120** (Luo et al. 2015). The fully fused diporphyrin **124** showed the major absorptions at 657 nm (log $\varepsilon = 5.05$) and 1322 nm (log $\varepsilon = 5.16$) and a HOMO–LUMO gap of 0.62 V. Anderson's group also reported similar oxidative fusion in the case of *meso*-triarylporphyrin **125** having a 9-anthracenyl group (Davis et al. 2010). The fully fused diporphyrin **126** showed intense absorptions at 665 nm (log $\varepsilon = 5.26$) and 1495 nm (log $\varepsilon = 5.16$) and a HOMO–LUMO gap of 0.77 V.

Ag^+-mediated *meso-meso* coupling of porphyrins and subsequent oxidative fusion leading to *β,β-*, *meso,meso-*, *β',β'*-triply fused multiporphyrins **128** with DDQ-$Sc(OTf)_3$ were originally developed by Osuka's group (Fig. 3.34) (Tsuda and Osuka 2001). Dimeric, trimeric, and tetrameric porphyrins show NIR absorption bands from 1100 to 1600 nm, and their 2PA cross section values (σ) were measured; 11,900 GM (λ_{ex} 1200 nm) for the dimer, 18,500 GM (λ_{ex} 2300 nm) for the trimer, and 41,200 GM (λ_{ex} 2300 nm) for the tetramer (Ahn et al. 2006; Nakamura et al. 2008).

As seen in many examples noted above, porphyrins show basic reaction behaviors characteristic of aromatic compounds, but unusual reaction behaviors were also observed probably due to macrocycle π-conjugation that stabilizes a radical state. Various organometallic transformations for modification of porphyrin structures have caused great developments in the porphyrin chemistry these days. It is well illustrated by the fact that photophysical and electrochemical properties can be fine-tuned to allow versatile applications as functional materials.

References

Adler AD, Longo FR, Finarelli JD, Goldmacher J, Assour J, Korsakoff L (1967) A simplified synthesis for meso-tetraphenylporphine. J Org Chem 32:476

Ahn TK, Kim KS, Kim DY, Noh SB, Aratani N, Ikeda C, Osuka A, Kim D (2006) Relationship between two-photon absorption and the π-conjugation pathway in porphyrin arrays through dihedral angle control. J Am Chem Soc 128:1700–1704

Akhigbe J, Brückner C (2013) Expansion of a pyrrole in meso-tetra-phenylporphyrin to a pyrazine imide moiety-using a beckmann rearrangement. Eur J Org Chem 3876−3884

Akhigbe J, Luciano M, Zeller M, Brückner C (2015) Mono- and bisquinoline-annulated porphyrins from porphyrin β,β'-dione oximes. J Org Chem 80:499−511
Banala S, Rühl T, Wurst K, Kräutler B (2009) "Blackening" porphyrins by conjugation with quinones. Angew Chem Int Ed 48:599–603
Barton DHR, Zard SZ (1985) A new synthesis of pyrroles from nitroalkenes. J Chem Soc Chem Commun 1098–1100
Bessho T, Zakeeruddin SM, Yeh C-Y, Diau EW-G, Grätzel M (2010) Highly efficient mesoscopic dye-sensitized solar cells based on donor-acceptor-substituted porphyrins. Angew Chem Int Ed 49:6646–6649
Bols PS, Anderson HL (2018) Template-directed synthesis of molecular nanorings and cages. Acc Chem Res 51:2083−2092
Borovkov VV, Lintuluoto JM, Inoue Y (1999) Synthesis of Zn-, Mn-, and Fe-containing mono- and heterometallated ethanediyl-bridged porphyrin dimers. Helv Chim Acta 82:919–934
Borovkov VV, Hembury GA, Inoue Y (2004) Origin, control, and application of supramolecular chirogenesis in bisporphyrin-based systems. Acc Chem Res 37:449–459
Bringmann G, Götz DCG, Gulder TAM, Gehrke TH, Bruhn T, Kupfer T, Radacki K, Braunschweig H, Heckmann A, Lambert C (2008) Axially chiral β,β'-bisporphyrins: synthesis and configurational stability tuned by the central metals. J Am Chem Soc 130:17812–17825
Brückner C, Rettig SJ, Dolphin D (1998) Formation of a meso-tetraphenylsecochlorin and a homoporphyrin with a twist. J Org Chem 63:2094–2098
Bruhn T, Witterauf F, Götz DCG, Grimmer CT, Würtemberger M, Radius U, Bringmann G (2014) C,C- and N,C-coupled dimers of 2-aminotetraphenylporphyrins: regiocontrolled synthesis, spectroscopic properties, and quantum-chemical calculations. Chem Eur J 20:3998–4006
Carvalho CMB, Brocksom TJ, de Oliveira KT (2013) Tetrabenzoporphyrins: synthetic developments and applications, Chem Soc Rev 42:3302–3317
Chumakov DE, Khoroshutin AV, Anisimov AV, Kobrakov KI (2009) Bromination of porphyrins (Review). Chem Heterocycl Comp 45:259–283
Collins HA, Khurana M, Moriyama EH, Mariampillai A, Dahlstedt E, Balaz M, Kuimova MK, Drobizhev M, Yang VXD, Phillips D, Rebane A, Wilson BC, Anderson HL (2008) Blood-vessel closure using photosensitizers engineered for two-photon excitation. Nat Photon 2:420–424
Collman JP, Gagne RR, Reed CA, Halbert TR, Lang G, Robinson WT (1975) Picket fence porphyrins. Synthetic models for oxygen binding hemoproteins. J Am Chem Soc 97:1427–1439
Crossley MJ, Burn PL (1991) An approach to porphyrin-based molecular wires: synthesis of a bis(porphyrin)tetraone and its conversion to a linearly conjugated tetrakisporphyrin system. J Chem Soc Chem Commun 1569–1571
Crossley MJ, King LG (1984) Novel heterocyclic systems from selective oxidation at the β-pyrrolic position of porphyrins. J Chem Soc Chem Commun 920–922
Crossley MJ, Burn PL, Langford SJ, Pyke SM, Stark AG (1991) A new method for the synthesis of porphyrin-α-diones that is applicable to the synthesis of trans-annular extended porphyrin systems. J Chem Soc Chem Commun 1567–1568
Daniell HW, Williams SC, Jenkins HA, Brückner C (2003) Oxidation of meso-tetraphenyl-2,3-dihydroxychlorin: simplified synthesis of β,β'-dioxochlorins. Tetrahedron Lett 44:4045–4049
Davis NKS, Thompson AL, Anderson HL (2010) Bis-anthracene fused porphyrins: synthesis, crystal structure, and near-IR absorption. Org Lett 12:2124−2127
Davis NKS, Thompson AL, Anderson HL (2011) A porphyrin fused to four anthracenes. J Am Chem Soc 133:30–31
Diev VV, Hanson K, Zimmerman JD, Forrest SR, Thompson ME (2010) Fused pyrene–diporphyrins: shifting near-infrared absorption to 1.5 μm and beyond. Angew Chem Int Ed 49:5523–5526
Dijkstra HP, ten Have R, van Leusen AM (1998) A direct synthesis of 2-(trimethylstannyl)pyrroles from Michael acceptors and stannylated tosylmethyl isocyanide. J Org Chem 63:5332–5338
Dolphin D (ed) (1978) The porphyrins. Academic Press, New York

Drobizhev M, Stepanenko Y, Rebane A, Wilson CJ, Screen TEO, Anderson HL (2006) Strong cooperative enhancement of two-photon absorption in double-strand conjugated porphyrin ladder arrays. J Am Chem Soc 128:12432−12433

Finikova O, Cheprakov A, Beletskaya I, Vinogradov S (2001) An expedient synthesis of substituted tetraaryltetrabenzoporphyrins. Chem Commun 261–262

Finikova O, Cheprakov A, Beletskaya I, Carroll P, Vinogradov S (2004) Novel versatile synthesis of substituted tetrabenzoporphyrins. J Org Chem 69:522–535

Fujimoto K, Osuka A (2018) A 1,5-naphthyridine-fused porphyrin dimer: intense nir absorption and facile redox interconversion with its reduced congener. Chem Eur J 24:6530–6533

Fujimoto K, Yorimitsu H, Osuka A (2014) Facile preparation of β-haloporphyrins as useful precursors of β-substituted porphyrins. Org Lett 16:972−975

Fukui N, Fujimoto K, Yorimitsu H, Osuka A (2017) Embedding heteroatoms: an effective approach to create porphyrin-based functional materials. Dalton Trans 46:13322–13341

Götz DCG, Gehrold AC, Dorazio SJ, Daddario P, Samankumara L, Bringmann G, Brückner C, Bruhn T (2015) Indaphyrins and indachlorins: optical and chiroptical properties of a family of helimeric porphyrinoids. Eur J Org Chem 3913–3922

Grzybowski M, Skonieczny K, Butenschçn H, Gryko DT (2013) Comparison of oxidative aromatic coupling and the Scholl reaction. Angew Chem Int Ed 52:9900–9930

Hata H, Shinokubo H, Osuka A (2005) Highly regioselective Ir-Catalyzed β-borylation of porphyrins via C−H bond activation and construction of β−β-linked diporphyrin. J Am Chem Soc 127:8264–8265

Huang X, Rickman BH, Borhan B, Berova N, Nakanishi K (1998) Zinc porphyrin tweezer in host−guest complexation: determination of absolute configurations of diamines, amino acids, and amino alcohols by circular dichroism. J Am Chem Soc 120:6185–6186

Ito S, Murashima T, Uno H, Ono N (1998) A new synthesis of benzoporphyrins using 4,7-dihydro-4,7-ethano-2H-isoindole as a synthon of isoindole. Chem Commun 1661–1662

Ito S, Uno H, Murashima T, Ono N (2001) Synthesis of benzoporphyrins functionalized with octaester groups. Tetrahedron Lett 42:45–47

Ito S, Hiroto S, Lee S, Son M, Hisaki I, Yoshida T, Kim D, Kobayashi N, Shinokubo H (2015) Synthesis of highly twisted and fully π-conjugated porphyrinic oligomers. J Am Chem Soc 137:142–145

Ito S, Hiroto S, Ousaka N, Yashima E, Shinokubo H (2016) Control of conformation and chirality of nonplanar π-conjugated diporphyrins using substituents and axial ligands. Chem Asian J 11:936–942

Jaquinod L, Siri O, Khoury RG (1998) Linear fused oligoporphyrins: potential molecular wires with enhanced electronic communication between bridged metal ions. Chem Commun 1261–1262

Jeandon C, Ruppert R (2011) A porphyrin with two coordination sites: the biquinoline ligand as a new potential external chelate. Eur J Org Chem 4098−4102

Jiang L, Zaenglein RA, Engle JT, Mittal C, Hartley CS, Ziegler CJ, Wang H (2012) Water-soluble ionic benzoporphyrins. Chem Commun 48:6927–6929

Kadish KM, Smith KM, Guilard R (eds) (2000) The porphyrin handbook. Academic Press, San Diego

Kadish KM, Smith KM, Guilard R (eds) (2010) Handbook of porphyrin science. World Scientific, Singapore

Kondratuk DV, Sprafke JK, O'Sullivan MC, Perdigao LMA, Saywell A, Malfois M, O'Shea JN, Beton PH, Thompson AL, Anderson HL (2014) Vernier-templated synthesis, crystal structure, and supramolecular chemistry of a 12-porphyrin nanoring. Chem Eur J 20:12826–12834

Kuimova MK, Botchway SW, Parker AW, Balaz M, Collins HA, Anderson HL, Suhling K, Ogilby PR (2009) Imaging intracellular viscosity of a single cell during photoinduced cell death. Nat Chem 1:69–73

Kumar S, Jiang X, Shan W, Jinadasa RGW, Kadish KM, Wang H (2018) β-Functionalized trans-A2B2 push–pull tetrabenzoporphyrins. Chem Commun 54:5303–5306

Kuroda Y, Kato Y, Higashioji T, Hasegawa J, Kawanami S, Takahashi M, Shiraishi N, Tanabe K, Ogoshi H (1995) Chiral amino acid recognition by a porphyrin-based artificial receptor. J Am Chem Soc 117:10950–10958

Kurotobi K, Kim KS, Noh SB, Kim D, Osuka A (2006) A quadruply azulene-fused porphyrin with intense near-IR absorption and a large two-photon absorption cross section. Angew Chem Int Ed 45:3944–3947

Kurotobi K, Toude Y, Kawamoto K, Fujimori Y, Ito S, Chabera P, Sundström V, Imahori H (2013) Highly asymmetrical porphyrins with enhanced push-pull character for dye-sensitized solar cells. Chem Eur J 19:17075–17081

Lewtaka JP, Gryko DT (2012) Synthesis of π-extended porphyrins via intramolecular oxidative coupling. Chem Commun 48:10069–10086

Lindsey JS (2010) Synthetic routes to meso-patterned porphyrins. Acc Chem Res 43:300–311

Lindsey J (1980) Increased yield of a desired isomer by equilibriums displacement on binding to silica gel, applied to meso-tetrakis(o-aminophenyl)porphyrin. J Org Chem 45:5215

Lindsey JS, Schreiman IC, Hsu HC, Kearney PC, Marguerettaz AM (1987) Rothemund and Adler-Longo reactions revisited: synthesis of tetraphenylporphyrins under equilibrium conditions. J Org Chem 52:827–836

Li X, Tanasova M, Vasileiou C, Borhan B (2008) Fluorinated porphyrin tweezer: a powerful reporter of absolute configuration for erythro and threo diols, amino alcohols, and diamines. J Am Chem Soc 130:1885–1893

Luo J, Lee S, Son M, Zheng B, Huang K-W, Qi Q, Zeng W, Li G, Kim D, Wu J (2015) N-annulated perylene-substituted and fused porphyrin dimers with intense near-infrared one-photon and two-photon absorption. Chem Eur J 21:3708–3715

Mandoj F, Nardis S, Pudi R, Lvova L, Fronczek FR, Smith KM, Prodi L, Genovese D, Paolesse R (2013) β-pyrazino-fused tetrarylporphyrins. Dyes Pigm 99:136–143

Mathew S, Yella A, Gao P, Humphry-Baker R, Curchod BFE, Ashari-Astani N, Tavernelli I, Rothlisberger U, Nazeeruddin MdK, Grätzel M (2014) Dye-sensitized solar cells with 13% efficiency achieved through the molecular engineering of porphyrin sensitizers. Nat Chem 6:242–247

McCarthy JR, Hyland MA, Brückner C (2004) Synthesis of indaphyrins: meso-tetraarylsecochlorin-based porphyrinoids containing direct o-phenyl-to-β-linkages. Org Biomol Chem 2:1484–1491

Meindl A, Plunkett S, Ryan AA, Flanagan KJ, Callaghan S, Senge MO (2017) Comparative synthetic strategies for the generation of 5,10- and 5,15-substituted push-pull porphyrins. Eur J Org Chem 3565–3583

Mikhaylov A, Kondratuk DV, Cnossen A, Anderson HL, Drobizhev M, Rebane A (2016) Cooperative enhancement of two-photon absorption in self-assembled zinc-porphyrin nanostructures. J Phys Chem C 120:11663−11670

Mizuno Y, Aida T, Yamaguchi K (2000) Chirality-memory molecule: crystallographic and spectroscopic studies on dynamic molecular recognition events by fully substituted chiral porphyrins. J Am Chem Soc 122:5278–5285

Mizuno Y, Alam MdA, Tsuda A, Kinbara K, Yamaguchi K, Aida T (2006) Hermaphroditic chirality of a D 2-symmetric saddle-shaped porphyrin in multicomponent spontaneous optical resolution: inclusion cocrystals with double-helical porphyrin arrays. Angew Chem Int Ed 45:3786–3790

Mysłiwiec D, Donnio B, Chmielewski PJ, Heinrich B, Stepien M (2012) Peripherally fused porphyrins via the Scholl reaction: synthesis, self-assembly, and mesomorphism. J Am Chem Soc 134:4822−4833

Nakamura Y, Jang SY, Tanaka T, Aratani N, Lim JM, Kim KS, Kim D, Osuka A (2008) Two-dimensionally extended porphyrin tapes: synthesis and shape-dependent two-photon absorption properties. Chem Eur J 14:8279–8289

Nishino N, Kobata K, Mihara H, Fujimoto T (1992) Efficient preparation of αβαβ-atropisomer of meso-tetra(o-aminophenyl)porphyrin. Chem Lett 1991–1994

Paolesse R, Jaquinod L, Sala FD, Nurco DJ, Prodi L, Montalti M, Natale CD, D'Amico A, Carlo AD, Lugli P, Smith KM (2000) *β*-Fused oligoporphyrins: a novel approach to a new type of extended aromatic system. J Am Chem Soc 122:11295–11302

Pawlicki M, Collins HA, Denning RG, Anderson HL (2009) Two-photon absorption and the design of two-photon dyes. Angew Chem Int Ed 48:3244–3266

Rao PD, Dhanalekshmi S, Littler BJ, Lindsey JS (2000) Rational syntheses of porphyrins bearing up to four different meso substituents. J Org Chem 65:7323–7344

Ravikanth M, Strachan J-P, Li F, Lindsey JS (1998) Trans-substituted porphyrin building blocks bearing iodo and ethynyl groups for applications in bioorganic and materials chemistry. Tetrahedron 54:7721–7734

Richeter S, Jeandon C, Kyritsakas N, Ruppert R, Callot HJ (2003) Preparation of six isomeric bis-acylporphyrins with chromophores reaching the near-infrared via intramolecular Friedel−Crafts reaction. J Org Chem 68:9200–9208

Rickhaus M, Jentzsch AV, Tejerina L, Grübner I, Jirasek M, Claridge TDW, Anderson HL (2017) Single-acetylene linked porphyrin nanorings. J Am Chem Soc 139:16502−16505

Rothemund P (1935) Formation of porphyrins from pyrrole and aldehydes. J Am Chem Soc 57:2010–2011

Ryan A, Gehrold A, Perusitti R, Pintea M, Fazekas M, Locos OB, Blaikie F, Senge MO (2011) Porphyrin dimers and arrays. Eur J Org Chem 5817–5844

Ryppa C, Senge MO, Hatscher SS, Kleinpeter E, Wacker P, Schilde U, Wiehe A (2005) Synthesis of mono- and disubstituted porphyrins: A- and 5,10-A2-type systems. Chem Eur J 11:3427–3442

Sahoo AK, Mori S, Shinokubo H, Osuka A (2006) Facile peripheral functionalization of porphyrins by Pd-catalyzed [3+2] annulation with alkynes. Angew Chem Int Ed 45:7972–7975

Samankumara LP, Dorazio SJ, Akhigbe J, Li R, Nimthong-Roldán A, Zeller M, Brückner C (2015) Indachlorins: nonplanar indanone-annulated chlorin analogues with panchromatic absorption spectra between 300 and 900 nm. Chem Eur J 21:11118–11128

Senge MO (2011) Stirring the porphyrin alphabet soup-functionalization reactions for porphyrins. Chem Commun 47:1943–1960

Senge MO, Shaker YM, Pintea M, Ryppa C, Hatscher SS, Ryan A, Sergeeva Y (2010) Synthesis of meso-substituted ABCD-type porphyrins by functionalization reactions. Eur J Org Chem 237–258.

Senge MO, Fazekas M, Pintea M, Zawadzka M, Blau WJ (2011) 5,15-A2B2-and 5,15-A2BC-type porphyrins with donor and acceptor groups for use in nonlinear optics and photodynamic therapy. Eur J Org Chem 5797–5816

Sessler JL, Mozaffari A, Johnson MR (1992) 3,4-Diethylpyrrole and 2,3,7,8,12,13,17,18-octaethylporphyrin [Pyrrole, 3,4-diethyl and 21H,23H-porphine, 2,3,7,8,12,13,17,18-octaethyl-]. Org Syn 70:68–72

Sessler JL, Gross Z, Furuta H (eds) (2017) Expanded, contracted, and isomeric porphyrins, a thematic issue. Chem Rev 117:2201–3881

Sprafke JK, Kondratuk DV, Wykes M, Thompson AL, Hoffmann M, Drevinskas R, Chen W-H, Yong CK, Kärnbratt J, Bullock JE, Malfois M, Wasielewski MR, Albinsson B, Herz LM, Zigmantas D, Beljonne D, Anderson HL (2011) Belt-shaped π-systems: relating geometry to electronic structure in a six-porphyrin nanoring. J Am Chem Soc 133:17262−17273

Sternberg ED, Dolphin D (1998) Porphyrin-based photosensitizers for use in photodynamic therapy. Tetrahedron 54:4151–4202

Sugiura K, Tanaka H, Matsumoto T, Kawai T, Sakata Y (1999) A Mandala-patterned Bandanna-shaped porphyrin oligomer, $C_{1244}H_{1350}N_{84}Ni_{20}O_{88}$, having a unique size and geometry. Chem. Lett. 1193–1194

Takahashi R, Kobuke Y (2005) Hexameric and pentameric slipped-cofacial dimers: toward an artificial light-harvesting complex. J Org Chem 70:2745–2753

Tsuda A, Osuka A (2001) Fully conjugated porphyrin tapes with electronic absorption bands that reach into infrared. Science 293:79–82

Uno H, Ito S, Wada M, Watanabe H, Nagai M, Hayashi A, Murashima T, Ono N (2000) Synthesis and structures of pyrroles fused with rigid bicyclic ring systems at β-positions. J Chem Soc Perkin Trans 1:4347–4355

Uno H, Nakamoto K-i, Kuroki K, Fujimoto A, Ono N (2007) Synthesis of porphyrin dimers fused with a benzene unit. Chem Eur J 13:5773–5784

Uoyama H, Kim KS, Kuroki K, Shin J-Y, Nagata T, Okujima T, Yamada H, Ono N, Kim D, Uno H (2010) Highly pure synthesis, spectral assignments, and two-photon properties of cruciform porphyrin pentamers fused with benzene units. Chem Eur J 16:4063–4074

van Leusen D, van Echten E, van Leusen AM (1992) Chemistry of sulfonylmethyl isocyanides. 37. Synthesis of 3,4-disubstituted pyrroles bearing substituents of electron-withdrawing and/or electron-donating nature. J Org Chem 57:2245–2249

Yella A, Lee H-W, Tsao HN, Yi C, Chandiran AK, Nazeeruddin MK, Diau EW-G, Yeh C-Y, Zakeeruddin SM, Grätzel M (2011) Porphyrin-sensitized solar cells with cobalt (II/III)–based redox electrolyte exceed 12 percent efficiency. Science 334:629–634

Yella A, Mai C-L, Zakeeruddin SM, Chang S-N, Hsieh C-H, Yeh C-Y, Angew MG (2014) Molecular engineering of push-pull porphyrin dyes for highly efficient dye-sensitized solar cells: the role of benzene spacers. Chem Int Ed 53:2973–2977

Zaidi SHH, Fico RM Jr, Lindsey JS (2006) Investigation of streamlined syntheses of porphyrins bearing distinct meso substituents. Org Process Res Dev 10:118–134